



Magnetostratigraphic correlations of Permian–Triassic marine-to-terrestrial sections from China

J.M.G. Glen^{a,b,*}, S. Nomade^{a,c}, J.J. Lyons^d, I. Metcalfe^e, R. Mundil^a, P.R. Renne^a

^aBerkeley Geochronology Center, 2455 Ridge Rd., Berkeley, CA 94709, USA

^bUS Geological Survey, MS 989, 345 Middlefield Road, Menlo Park, CA 94025, USA

^cLaboratoire des Sciences du Climat et de l'Environnement, (CEA-CNRS-UVSQ), Orme des Merisiers, F-91191 Gif sur Yvette Cedex, France

^dDepartment of Earth Sciences, University of California Santa Cruz, CA 95064, USA

^eSchool of Environmental and Rural Science, University of New England, Armidale NSW 2351, Australia

ARTICLE INFO

Article history:

Received 14 January 2008

Received in revised form 24 November 2008

Accepted 4 March 2009

Keywords:

Permian–Triassic boundary

China

Magnetostratigraphy

Marine

Non-marine

Paralic

ABSTRACT

We have studied three Permian–Triassic (PT) localities from China as part of a combined magnetostratigraphic, ⁴⁰Ar/³⁹Ar and U–Pb radioisotopic, and biostratigraphic study aimed at resolving the temporal relations between terrestrial and marine records across the Permo–Triassic boundary, as well as the rate of the biotic recovery in the Early Triassic. The studied sections from Shangsi (Sichuan Province), Langdai (Guizhou Province), and the Junggar basin (Xinjiang Province), span marine, paralic, and terrestrial PT environments, respectively. Each of these sections was logged in detail in order to place geochronologic, paleomagnetic, geochemical, conodont and palynologic samples within a common stratigraphic context. Here we present rock-magnetic, paleomagnetic and magnetostratigraphic results from the three localities.

At Shangsi, northern Sichuan Province, we sampled three sections spanning Permo–Triassic marine carbonates. Magnetostratigraphic results from the three sections indicate that the composite section contains at least 8 polarity chrons and that the PT boundary occurs within a normal polarity chron a short distance above the mass extinction level and a reversed-to-normal (R–N) polarity reversal. Furthermore, the onset of the Illawarra mixed interval lies below the sampled section indicating that the uppermost Permian Changhsingian and at least part of the Wuchiapingian stages postdate the end of the Kiaman Permo–Carboniferous Reversed Superchron.

At Langdai, Guizhou Province, we studied magnetostratigraphy of PT paralic mudstone and carbonate sediments in two sections. The composite section spans an R–N polarity sequence. Section-mean directions pass a fold test at the 95% confidence level, and the section-mean poles are close to the mean PT pole for the South China block. Based on biostratigraphic constraints, the R–N transition recorded at Langdai is consistent with that at Shangsi and demonstrates that the PT boundary occurred within a normal polarity chron a short distance above the mass extinction level.

In the southern Junggar basin, Xinjiang Province, in northwest China, we determined the magnetostratigraphy of three sections of a terrestrial sequence. Normal and reversed polarity directions are roughly antipodal, and magnetostratigraphies from the three sections are highly consistent. Combined bio- and magneto-stratigraphy used to correlate this sequence to other PT sequences suggests that the previously-proposed biostratigraphic PT boundary in the Junggar sections was most likely misplaced by earlier workers suggesting that further work is necessary to confidently place the PT boundary there.

Published by Elsevier Ltd.

1. Introduction

The Permian–Triassic boundary marks the largest mass extinction in Earth's history when perhaps over 90% of marine life and 70% of terrestrial life was extinguished (Raup, 1979; Rohde and

Muller, 2005). Unfortunately, good records of this period are scant due to a near global stratigraphic break in records spanning that time. In virtually all records of the latest Permian to earliest Triassic there appears to be a lithologic change coincident with the biostratigraphic Permian–Triassic (PT) boundary, leading to uncertainties about the completeness of even the best records. Thus, questions about the timing and duration of this mass extinction, as well as the synchronicity of marine and terrestrial extinctions, have proven difficult to resolve.

* Corresponding author. Address: US Geological Survey, MS 989, 345 Middlefield Road, Menlo Park, CA 94025, USA. Tel.: +1 650 329 5282; fax: +1 650 329 5133.

E-mail address: jglen@usgs.gov (J.M.G. Glen).

The broader study, of which this is a part, entails a multidisciplinary paleomagnetic, $^{40}\text{Ar}/^{39}\text{Ar}$ and U–Pb isotopic-dating, biostratigraphic, and chemostratigraphic study of PT boundary sections in China that span marine-to-terrestrial paleo-environments. The aim of this research is to constrain the age and duration of extinctions and of biologic recovery in land and marine settings, and to determine the extent to which the end-Permian biotic crisis, or correlative isotopic anomalies, in the sea and on land were synchronous. In this paper, we report on magnetostratigraphic results from three Chinese PT-section localities (Fig. 1) from Shangsi (Sichuan Province), Langdai (Guizhou Province), and the Junggar basin (Xinjiang Province), that represent marine, paralic (terrestrial to shallow marine), and terrestrial environments, respectively.

1.1. PT biostratigraphic boundary definition

Recent biostratigraphic work at the global stratotype and parastatotype sections (GSSP) for the base of the Triassic at Meishan (Zhejiang Province, China) and Shangsi (Sichuan Province, China) respectively, recognizes several species of the conodont genus *Hindeodus* as key index species for identifying the PT boundary and transition level (Metcalf et al., 2001; Metcalfe et al., 2007; Nicoll et al., 2002). The first appearance of the Triassic species *Hindeodus parvus* is used (Yin et al., 1996) by the Subcommission on Triassic Stratigraphy and the International Union of Geological Sciences to define the boundary (Yin et al., 2001). We note that this boundary necessarily lies stratigraphically above the mass extinction level.

Although a Global Stratotype Section has been established for the PT boundary at Meishan, Changxing County, Zhejiang Province China (Yin et al., 2001), recent biostratigraphic studies (Metcalf et al., 2007; Nicoll et al., 2002) highlight ongoing problems of precise correlation of the PT boundary. Because radioisotopic-age, and

perhaps magnetostratigraphic controls are better constrained at Shangsi, and because Shangsi appears to be a more complete section, we suggest that Shangsi may represent a better type marine record of PT boundary time than Meishan.

In the non-marine environment, the PT boundary has long been considered by vertebrate paleontologists to be marked by the first appearance of *Lystrosaurus* (e.g., Lucas, 1998). More recent work has however demonstrated that the first appearance of *Lystrosaurus* in the Karoo basin is within a reversed magnetic polarity chron and that the last *Dicynodon* occurs higher than the first *Lystrosaurus* within the lower part of the succeeding normal polarity chron. The PT boundary is interpreted to be a little higher in the sequence within the same normal polarity chron (for further discussion see Metcalfe et al., this issue; Lucas, this issue). At Dalongkou, Junggar Basin, there is also an overlap between *Lystrosaurus* and *Dicynodon*, and this, combined with evidence from palynomorphs and conchostacans, suggests that the PT boundary location is still equivocal but probably located high in the Guodikeng Formation or in the lower part of the Jiucuiyuan Formation (see Metcalfe et al., this issue).

1.2. Causes for PT mass extinctions

Although the late Permian to early Triassic biotic transition was among the most dramatic events in the history of life on Earth, there has yet to emerge a clear picture of the causes and dynamics of this transition. Some argue that the PT boundary extinction was rapid, perhaps resulting from some combination of volcanically induced climate change (e.g., Courtillot et al., 1999; Courtillot and Renne, 2003; Renne et al., 1995), oceanic anoxia due to deep-water overturn (Wignall and Twitchett, 1996), hypercapnia (Knoll et al., 2007), melting of gas hydrates (Krull and Retallack, 2000; Ry-skin, 2003), large-scale marine regression and/or transgression

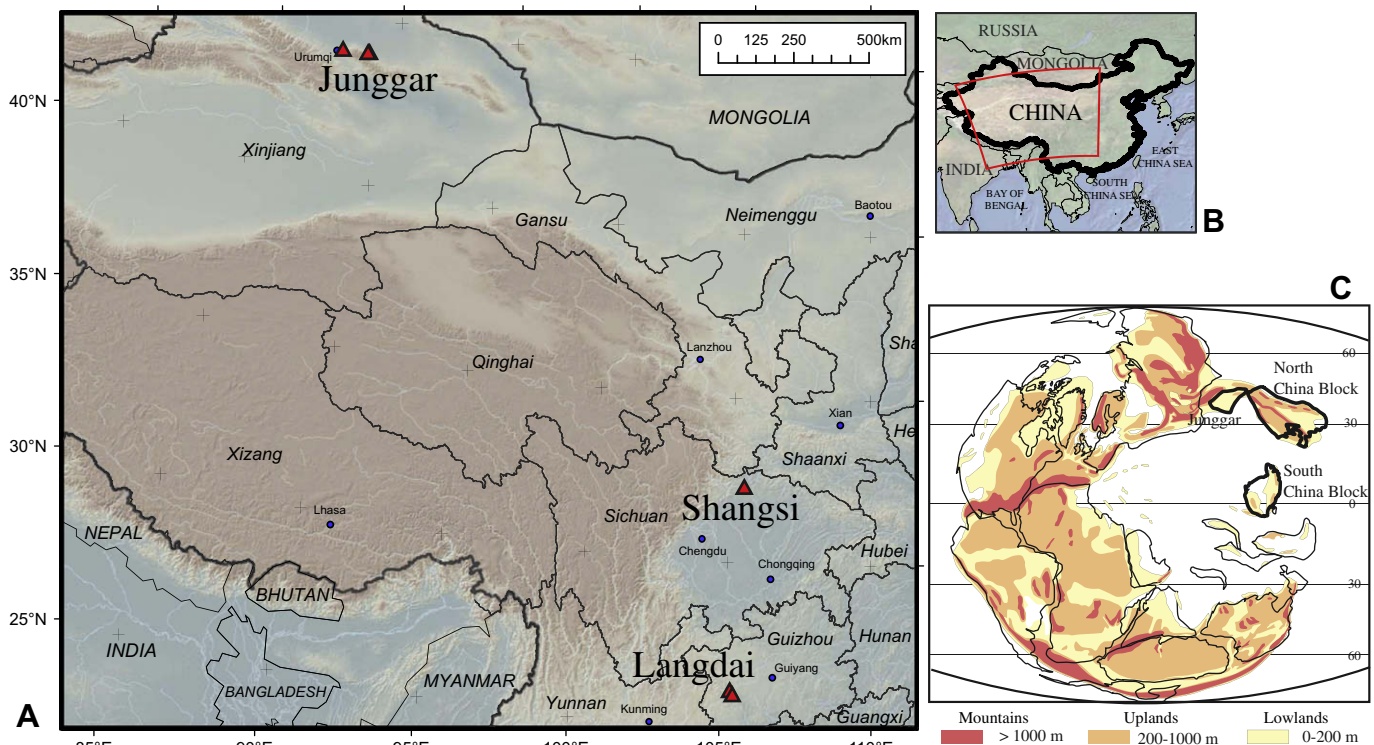


Fig. 1. (A) Map showing locations of sampled sections (red triangles) from the studied localities (Shangsi, Langdai, and Junggar), (B) Index map showing extent of area shown in A (red box), and (C) Permo-Triassic paleogeographic reconstruction (after Rees, 2002). (For interpretation of the references in colour in this figure legend, the reader is referred to the web version of this article.)

(Hallam and Wignall, 1999), and/or bolide impact (Becker et al., 2001; Hagstrum, 2005; Kaiho et al., 2001; Rampino, 1992; Xu and Yan, 1993), although evidence for the later is scarce (Farley et al., 2005; Glikson, 2004; Müller et al., 2005; Renne et al., 2004a; Wignall et al., 2004).

The close coincidence of the PT mass extinction with the eruption of the Siberian Traps (the main pulse of volcanism is constrained by $^{40}\text{Ar}/^{39}\text{Ar}$ to an age of 250 Ma; Reichow et al., 2002; Renne, 1995) is perhaps the most compelling argument for volcanism as a direct causal mechanism for the PT biotic crisis. Nonetheless, continued and vigorous discussion of this topic indicates that the issue has not yet been settled and highlights the need for further research. Because marine and non-marine environments may react at different times and in very different manners depending on the trigger of mass extinction, the relative timing of biotic change, isotopic shifts, and geochemical anomalies in marine and terrestrial sections may be crucial in distinguishing between different causal mechanisms.

1.3. Radio-isotopic age constraints on the PT boundary

Volcanic ash/clay layers were sampled at Shangsi and Langdai sections for both U–Pb and $^{40}\text{Ar}/^{39}\text{Ar}$ radio-isotopic dating, as part of this study. Radioisotopic results from this work are presented elsewhere (Mundil et al., 2004) and summarized here. Zircons and feldspars were extracted from the bentonite layers and dated using the IDTIMS method for U–Pb analyses and for single-grain laser-fusion $^{40}\text{Ar}/^{39}\text{Ar}$ analyses, respectively. Several U–Pb single zircon ages (using the CA-TIMS technique, Mattinson, 2005) from Shangsi and Meishan yield an age for the PT boundary that is slightly older than 252 Ma and suggest the extinction event was very rapid, spanning less than a few 100 ka (Mundil et al., 2004). It is important to note, however, that recent studies comparing U–Pb and $^{40}\text{Ar}/^{39}\text{Ar}$ data from the same rocks show that $^{40}\text{Ar}/^{39}\text{Ar}$ ages are systematically younger by 1% for Mesozoic times (the bias decreases with age), due most likely to miscalibrations of the ^{40}K decay constant and the age of the flux monitor (Min et al., 2000; Mundil et al., 2006b). This suggests that reported $^{40}\text{Ar}/^{39}\text{Ar}$ ages of ~ 250 Myr for the PT boundary, from the GSSP at Meishan (Renne et al., 1995) and Shangsi (Renne et al., 2004b), and for the main pulse of the Siberian Traps (Renne et al., 1995), are ~ 2.5 Ma too young. Taking this systematic bias into account, the 250 Ma $^{40}\text{Ar}/^{39}\text{Ar}$ age corresponds to a corrected age of ~ 252.5 Ma, in agreement with U–Pb data from Shangsi and Meishan (Mundil et al., 2004). An age in excess of 252 Ma is in contrast to a recent estimate of the age of the boundary of 251.0 ± 0.4 Ma (adopted by Wardlaw et al., 2004, for the most recent timescale compilation) that is based on previous U–Pb age data by Bowring et al. (1998) that have been shown to be inaccurate (Mundil et al., 2001).

The only PT boundary age data from tuffs in non-marine sections come from sections in the southwestern United States and eastern Australia that yield U–Pb ages of ~ 252 Ma (Chang et al., 2007; Mundil et al., 2006a). Biostratigraphic correlation with marine sections remains elusive; however, new magnetostratigraphic data (Chang et al., 2007) in combination with these age data may prove useful for future global correlations.

1.4. Correlating PT sections

China, which holds some of the most continuous PT sections known, presents a unique opportunity for comparing marine and non-marine PT sediments and assessing the timing of PT boundary events in marine and terrestrial environments. This cannot be done, however, without a means of precisely correlating geographically distant sections. Lithologic correlations of the boundary zone

have proven to be unreliable due to sedimentologic, tectonic, paleogeographic, and climatic differences between sections (Lozovsky, 1998). Biostratigraphic methods, however, promise a more accurate means of tying together disparate sections. It has been suggested that a reported fungal spike (Erwin, 1993) occurring at several PT boundary sites followed the widespread and rapid demise of vegetation at the mass extinction boundary, and represents the proliferation of fungi on large volumes of decaying plant matter. If so, the fungal bloom might have spanned a brief interval (less than 40,000 yrs) following the PT boundary event and could therefore be used to correlate marine and non-marine sections (Steiner et al., 2003). It has been shown (Foster et al., 2002), however, that the supposed fungal spores are likely algae remains which could not have acted as a metaboliser of dead vegetation resulting from the extinction event. In fact, these fossils are documented at stratigraphic levels ranging far from the PT boundary zone (spanning several million years) and well outside the time postulated for mass extinction, thus precluding them as marker horizons to indicate the PT boundary or to correlate remote PT sections.

Carbon isotope studies (e.g., Baud et al., 1989; Holser et al., 1989; Krull and Retallack, 2000; Morante, 1996; Payne et al., 2007; Wang et al., 1994; Wignall et al., 1998) show that a large negative shift in stable carbon isotopes in marine and non-marine records is associated with the PT boundary and can be used to correlate PT stratigraphy and to detect hiatuses in sedimentation, particularly in marine settings. Because the character of the isotopic excursions near the PT boundary are different in different environments and depending on the source of carbon analyzed, carbon isotopic studies are limited as a fine-scale correlation tool (for further discussion, see Metcalfe et al., this issue).

Magnetostratigraphy, on the other hand, may offer the greatest potential for correlating vastly different environments (marine and terrestrial) that are unlikely to contain the necessary biologic, lithologic, or chemical material for correlating all sections. Furthermore, a magnetic reversal, near the mass extinction level, could provide a globally synchronous horizon for linking PT sections.

1.5. Global PT boundary magnetostratigraphy

Global magnetostratigraphic compilations of PT boundary sections (e.g., Gallet et al., 2000; Nawrocki, 2004; Steiner, 2006; Szurlics et al., 2003) reveal that a majority of PT records places the mass extinction level within a reversed polarity chron or coincident with a reversed-to-normal (R–N) polarity transition and the biostratigraphic boundary within the lower part of the succeeding normal polarity chron. Nonetheless, notable discrepancies exist, with some records placing the biostratigraphic boundary within the normal chron slightly above the reversal boundary (e.g., Menning, 1995), while others place it coincident with the polarity transition (e.g., Steiner et al., 1989).

At Meishan, the PT boundary and the mass extinction event are placed within the normal magnetozone above the PT-proximal reversal (Li and Wang, 1989). Some indication, however, of the possible presence of the minerals goethite and hematite, which commonly occur as secondary minerals that can carry post-depositional magnetizations, casts some doubt on the reliability of the magnetic record derived from these sediments. This uncertainty is further supported by inconsistencies between the study of Li and Wang (1989) and more recent paleomagnetic results of Zhu and Liu (1999), which place the boundary within a short reversed polarity chron. The discrepancy between these two studies and with the majority of other PT records suggests that additional detailed rock-magnetic and magnetostratigraphic studies are required to determine whether a reliable paleomagnetic record can be obtained from the Meishan section.

Lower Triassic magnetostratigraphy has been reported by Steiner et al. (1989) for sections from Sichuan Province (China) that extend from the PT boundary to the upper part of the Lower Triassic (Spathian). Their results suggest that the Early Triassic spans nine polarity zones, the same number found for sections from the Canadian Arctic (Ogg and Steiner, 1991). Correlation of the Chinese and Arctic records, however, appears questionable based on biostratigraphy alone.

Numerous studies spanning the Late Permian (e.g., Haag and Heller, 1991 – Pakistan; Khramov, 1974 – Ural Mountains; Molina-Garza et al., 1989 – northern Texas) consistently reveal that the Late Permian spanned several (5–7) normal polarity chrons. None of these studies, however, adequately constrain the age of the Permo-Carboniferous Reversed Superchron (PCRS). The PCRS, also called the Kiama Superchron, is a 40 m.y.-long period of dominantly reversed polarity that ended sometime in the Late Permian with what has been called the Illawarra reversal (Irving and Parry, 1963); a feature that is commonly used to correlate Permian sections. Despite the obvious importance of a well-constrained age for this reversal, no reliable ages spanning it have been obtained to date for correlation purposes.

The work presented here represents the first multi-disciplinary approach to map the chronostratigraphy of biotic, isotopic and chemical changes across the PT using magnetostratigraphy and radioisotopic geochronologic methods. Furthermore, because this work involves sampling of some of the most continuous PT boundary sections in marine, terrestrial and paralic environments, it has the unique potential to address the relative timing of onshore and offshore changes.

2. Methods

2.1. Sampling

Most samples (taken using a gasoline-powered drill) were oriented using magnetic and sun compasses. Cores of 2.5 cm diameter were later cut into 2.2 cm long specimens for performing paleo- and rock-magnetic measurements. In less consolidated material that was difficult to drill, hand samples were taken and oriented with a magnetic compass. Hand samples were later sub-sampled in the laboratory to yield 1 cm³ cubic specimens for measurement. Sampling density within each section varied depending on the quality of the outcrop and the position within the section. In general, finer-grained material was preferentially sampled and the highest density sampling performed near the expected PT boundary.

2.2. Rock magnetic measurements

Rock magnetic measurements were made to aid interpretations of sample demagnetization behavior, constrain the magnetic mineralogy, and assess the quality of magnetic records. We performed susceptibility versus temperature (K–T), isothermal remanent magnetization (IRM), and Lowrie 3-axis IRM/thermal demagnetization experiments (Lowrie, 1990) using facilities at U.C. Santa Cruz (UCSC) and the Berkeley Geochronology Center (BGC). Low-field magnetic susceptibility versus temperature (25–700°C) experiments were made on powdered samples (from all three localities) in argon with an AGICO KLY-2 Kappabridge equipped with a CS-2 furnace. A Princeton Instruments MicroMag AGFM was utilized for some isothermal remanent magnetization (IRM) acquisition experiments that were performed on small (~200 mg) rock chips (from Shangsi and Langdai localities). We also performed IRM experiments on whole (11 cm³) specimens (from Shangsi and Junggar localities) using an ASC Scientific (ASC) impulse magne-

tizer. We determined Curie temperatures from our K–T data using the technique of Prevot et al. (1983). Rock magnetic results are presented in Appendices A and B.

2.3. Remanent magnetization

Remanent magnetization measurements were made in shielded rooms at the BGC and UCSC paleomagnetism laboratories using 2G Enterprises cryogenic magnetometers. We applied both stepwise thermal (the principal method applied) and alternating field (AF) demagnetization (generally consisting of more than 15 steps) to samples to determine characteristic and overprint components of magnetization. AF demagnetizations were performed with 2G two-axis and Sapphire Instruments AF demagnetizers, and thermal demagnetizations were carried out in air in ASC and UCSC-in-house built shielded furnaces. In general, we found very good agreement between AF and thermal results, though thermal demagnetization was generally more effective for removing strong present day field (PDF) overprints and for revealing high-stability secondary overprints.

Characteristic components of magnetization (ChRM) were derived using least squares principal component analysis (Kirschvink, 1980). For the determination of mean paleomagnetic directions and confidence circles, we used Fisher (1953) statistics as modified by McFadden and McElhinny (1988) for the inclusion of great circle data. Fold tests were applied following the method of McFadden (1990) and reversal tests following the method of McFadden and McElhinny (1990).

2.4. Polarity determination

Sample characteristic remanent directions for the stable endpoint magnetizations were determined by fitting lines to at least three successive demagnetization steps. We determined polarity from the great circle demagnetization data by fitting great circles to at least three points of the demagnetization data and determining if that great circle path, with increasing levels of demagnetization, trended toward the expected normal or reversed polarity direction.

Depending on the strength of the overprints and stability of the primary magnetizations, the demagnetization results were divided into three groups: stable endpoint magnetizations, great circle trends, and unstable or completely overprinted magnetizations. Sample magnetization data were accepted or rejected based on the criteria discussed below.

Although many of the samples yielded good quality data that allowed a straightforward determination of polarity, determining polarity from some samples was difficult due to unstable magnetizations, complete PDF overprints, or strong high-stability secondary overprints. Samples with clearly unstable demagnetization behavior were simply discarded. Determining which of the data were excessively influenced by the present field or by high-stability secondary overprints was more difficult, as there is a variable degree to which these magnetization directions succeed in reaching the expected PT direction. To determine if sample data were usable, we considered the angular distance between best-fit directions or great circles, and PDF and PT reference directions [i.e., reference directions of Yang and Besse (2001) for Shangsi and Langdai localities, and Nie et al. (1993) for the Junggar locality]. We considered directions to be excessively influenced by secondary overprints and did not use them to determine locality mean directions and magnetostratigraphy, if (1) best-fit directions (or the last point used to fit great circles) were within an angular distance (A) from the PF direction (where A is 25% of the angular distance between PF and expected direction) and, (2) if great circles did not trend to within 25° of the expected direction. Some sam-

ples for the Shangsi sections that did not fully meet these criteria, but which we still considered may yield reliable information on sample polarity, were used to help guide interpretation of section magnetostratigraphies.

3. Shangsi marine sections, Sichuan Province

At Shangsi, northern Sichuan Province, in the Longmenshan Indosinian folded zone of the Qinling fold system, we have sampled two nearby parallel sections, and a third section that lies within the opposing limb of an anticline (Fig. 2). Earlier magnetostratigraphic studies at Shangsi indicate that the locality contains at least six polarity chrons and that the PT boundary likely corresponds with, or shortly precedes, an R-N polarity transition (Heller et al., 1988; Steiner et al., 1989). These earlier studies, however, lacked both a fold test and multiple sections that could corroborate the magnetostratigraphic results and test the reliability of remanence. In addition, because these studies did not sample a 3 m zone of friable, silty sediments occurring immediately above the extinc-

tion level, they were unable to determine the precise position of the boundary with respect to the nearby polarity reversal. The present study involves detailed paleomagnetic sampling of multiple sections to address lingering questions regarding the reliability of the magnetostratigraphic record, and to accurately place magnetostratigraphic, biostratigraphic, geochronologic and chemostratigraphic samples within a common stratigraphic and temporal framework.

3.1. Geologic setting

Some of the most continuous marine records of the PT boundary occur at Shangsi, where the Wujiaping, Dalong and Feixianguan formations comprise a sequence of marine limestones and shales that span the late Permian and early Triassic (Lai et al., 1986b, 1996; Wignall et al., 1995; Yang et al., 1987). These sediments, which were deposited on the Yangtze platform, presently crop out in the Longmenshan Indosinian folded zone of the Qinling fold belt along the northern margin of the Yangtze block (Figs. 1 and 2).

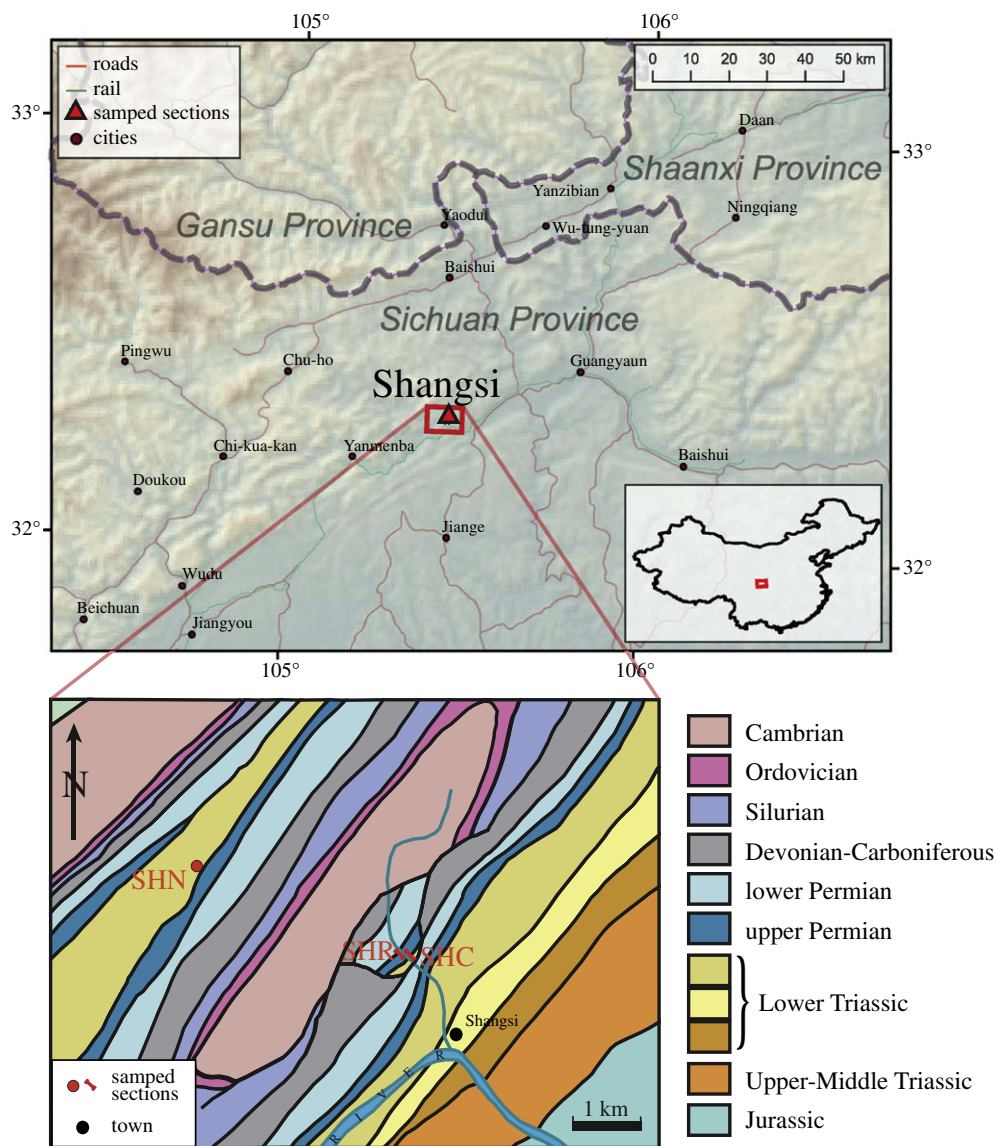


Fig. 2. Index map showing location of sampled Shangsi sections (Sichuan Province). Section labels refer to SHR – Road section, SHC – Creek section (main), and SHN – Northwest limb section. Road (SHR) and Creek (SHC) sections occur on the southeast limb of a northeast-trending anticline. Section SHN lies to the northwest on the opposing limb.

The PT biostratigraphic boundary has been placed approximately 1 m above the boundary between the Dalong and Feixianguan formations (Lai et al., 1996). Recent conodont biostratigraphic studies and graphic correlation suggest a similar placement (Metcalf et al., 2007).

The Wujiaping Formation (58 m thick), which comprises the lower portion of the Shangsi stratigraphy, consists primarily of thick-bedded limestones and is marked by a coal seam at its base. The overlying Dalong Formation (42 m thick) comprises medium-bedded limestones overlain by thin interbeds of limestone and shale. The Feixianguan Formation (61 m of sampled section) has an 8 m thick zone of mudstone and shale at its base, which contains the PT boundary interval, and overlying medium to thinly bedded limestones, micritic limestones, shales and marl. For a detailed stratigraphic description of the Shangsi locality, see Metcalfe et al. (2003) and Metcalfe and Nicoll (2007).

We sampled three sections of the Shangsi stratigraphy that provide duplicate parallel sequences and the possibility of performing a fold test. The main section, exposed in a creek bed at Shangsi near the city of Guangyuan, is situated on the southeast limb of an anticline trending 40° (SHC, Fig. 2). A parallel though less complete section, sampled along a road ~25–150 m above the main section (SHR, Fig. 2), coincides with sampling performed by previous workers (Heller et al., 1988; Steiner et al., 1989). The third, apparently condensed, section having a lower accumulation rate was taken ~3.5 km to the northwest on the opposing limb of the anticline (SHN, Fig. 2).

We sampled at roughly 1 m intervals throughout the sections, and more closely near the boundary, collecting a total of 286 cores and nine oriented hand samples from the three sections that span over 170 m of composite stratigraphy from the base of the Wujiaping Formation up through the Feixianguan Formation. Oriented hand samples were taken from a poorly consolidated clastic zone of silt and mudstones lying immediately above the mass-extinction level. This was necessary because the sediment was too friable to sample by drilling, which most likely accounts for why previous sampling efforts by Heller et al. (1988) and Steiner et al. (1989) did not recover material from these lowermost Triassic detrital sediments.

Average dips of the beds were 48° and 46° for the northwest and southeast limbs respectively. Within a <20 m deformed zone in the Feixianguan Formation, however dips varied significantly from the section mean, ranging from 16° to 64°. The overall strike of beds is 40° and 223° for the northwest and southeast limbs, respectively.

3.2. Biostratigraphy

Biostratigraphic studies of the Shangsi sections (Metcalf et al., 2007; Nicoll et al., 2002) indicate that the first occurrence of *Hindeodus parvus* is 4.5 m above the major lithologic boundary between Dalong and Feixianguan formations that marks a disruption of carbonate deposition by the accumulation of siltstones and mudstones. The occurrence of *Hindeodus chanxingensis* Wang, and graphic correlation however suggest that the PT boundary lies closer (within 1 m) to the formation boundary (Metcalf et al., 2007). The transition from carbonate to mud deposition also corresponds with the stratigraphically highest observed typical Permian fauna, and with what is believed to be the mass extinction level. Limited conodont control suggests that the northwest limb lies entirely above the biostratigraphic boundary.

3.3. Rock magnetic results

The majority of the Shangsi samples are weakly magnetic and have low initial magnetic susceptibilities [average natural

remanent magnetization (NRM) magnetization was 1.83×10^{-4} A/m, and average initial susceptibility was 1.9×10^{-5} SI].

K–T data often show flat heating curves up to 350–400 °C, followed by a bump in susceptibility that peaks in the range of 350–550 °C (Appendix A1). Significant drops in susceptibility, with inflections between 550 and 580 °C suggest the presence of magnetite. Cooling curves generally display large increases in susceptibility that indicate chemical reactions occur upon heating, due likely to the oxidation of pyrite to magnetite. AF-demagnetization results reveal that the majority of samples have a magnetic mineralogy dominated by a soft magnetic mineral. Data from Lowrie 3-axis IRM thermal demagnetization experiments indicate that sample magnetizations reach substantial saturation at low applied fields (0.12 T) and that remanence is dominated by a low-coercivity, high intensity magnetization mineral, such as titanomagnetite, that is largely destroyed by 550 °C (Appendix B1). Below 450 °C, directional data from these tests show that the composite magnetization direction of these artificially magnetized samples remained close to the direction of the softest IRM axis.

Medium bedded limestones and thin interbedded limestone and mudstone units within the Dalong Formation contain organic material that may have formed in place or was derived elsewhere, such as the coal seam at the base of the sampled portion of the Wujiaping Formation, and subsequently migrated into the bedded units higher in the section. In either case, reducing conditions associated with petroleum formation may have effected the remanence signal in this portion of the section. Indeed, the majority of samples that yielded directions which were considered unreliable (see discussion below) came from this part of the stratigraphy.

Titanomagnetite is most likely the primary carrier of magnetization. It is therefore likely that the sediments carry a stable primary remanence. However, a significant presence of pyrite in some samples, especially low in the stratigraphic section, is of some concern as it could reflect post-depositional reduction accompanied by the destruction of primary magnetic carriers like magnetite and even the generation of new magnetic material in the form of iron sulfides. Iron sulfides, such as greigite or pyrrhotite, may indeed be present as a second phase characterized by moderate to high coercivities and moderate unblocking temperatures (300–400 °C).

3.4. Magnetic remanence results

We applied stepwise thermal demagnetization consisting of roughly 15 steps in order to determine characteristic components of magnetization. Results from the parallel sections are in close agreement, and confirm the principal magnetozones of Heller et al. (1988), indicating that the magnetostratigraphy can be reliably reproduced within the section.

In order to determine the magnetic stratigraphy, we stepwise AF and thermally demagnetized over 300 specimens from the three sections. AF and thermal demagnetization yielded similar results, but thermal demagnetization was generally more effective at removing secondary overprints. Natural remanent magnetization directions from all sections cluster around the PDF direction in geographic coordinates and scatter after applying a bedding correction (Appendix C1), indicating that the NRM directions reflect the presence of a post-folding PDF overprint.

Although sample magnetizations carry, in some cases, a significant overprint component, both normal and reversed stable end-points were isolated from samples in all three sections. In many cases, however, directions had to be inferred from great circle analysis.

Demagnetization data reveal that a presumably viscous overprint of north and down disappeared by between 200 °C and 250 °C, after which sample magnetizations of both polarities

decayed linearly toward the origin (Appendix D1) up to between 300 °C and 400 °C. Above 450 °C to 500 °C, these magnetizations often became unstable or trended toward anomalous directions.

We limited our interpretation of the sample demagnetization data to the range below which spurious magnetizations are observed (~400 °C) due to an unstable primary remanence or chemical alterations. The stable endpoint directions determined from the sample data below this temperature appear to be primary directions since, as discussed below, they are consistent with the PT direction derived from the reference pole for the South China block, and reversed and normal polarity directions are roughly antipodal.

Based on the criteria and methods discussed above, we accepted and determined polarity from 114 of the 301 measured samples (Appendix G1). While many of the Shangsi samples allowed a straightforward determination of polarity, some, particularly from the lower portion of the sampled stratigraphy, yielded spurious results. Samples, from a roughly 30 m zone in the lower half of the sampled section, containing significant amounts of organic material yielded directions that were unstable or close to the present or geocentric axial dipole field direction, suggesting that they had undergone post-folding remagnetization, likely associated with the presence of hydrocarbons.

Secondary overprinting, though varied, was observed to some degree at horizons scattered throughout the section, often leading to demagnetizations that failed to fully reach the expected PT direction. In these cases polarity determinations were made from demagnetization curves based on a comparison of the expected PT direction derived from the reference pole for the South China block (Yang and Besse, 2001).

In the majority of cases where sample magnetizations did not attain stable endpoints, magnetization data did, however, trend along stable two-component great circles between the PDF overprint direction and a ChRM that is consistent with the expected PT direction (Appendix E1). In general, these great circle magnetizations were stable over a temperature range similar to those magnetizations that attained stable endpoints (350–450 °C). In addition, the great circle paths roughly trend toward the same directions that were attained by the stable endpoint magnetizations discussed above (Fig. 3).

Samples that displayed unstable behavior during demagnetization or were significantly overprinted by the present-day field were considered unreliable and were not used for polarity determinations. Samples from the Dalong Formation that contained significant organic material, generally had lower NRM intensities and lower initial susceptibilities perhaps rendering them more susceptible to PDF overprints. Additionally, the oxidation of pyrite to magnetite may be responsible for the spurious demagnetization behavior observed in some cases, as this reaction disrupted the sample magnetizations before they attained stable endpoints.

We accepted demagnetization data, which included stable endpoint magnetizations and great circle trends, from 42 samples. An additional 35 samples, yielding great circle trends that did not fit the full selection criteria but displayed distinctive trends towards either the normal or reversed expected PT direction, were used to help determine polarity. The remainder of the data was discarded due to unstable demagnetization behavior, complete present field overprints, or other high-stability secondary overprints.

Accepted line and great circle fits to the demagnetization data (Appendices F1, G1, H1) were combined to yield mean normal and reversed directions that are roughly antipodal. A fold test performed on mean directions from both primary (SHC&SHR, Fig. 2) and alternate (SHN, Fig. 2) sections, however, was inconclusive due to the fact that the shallow northeast ChRM lies very close to the trend of the regional fold axis. Nonetheless, directions and great circles (Fig. 3, Appendix F1), and the Shangsi locality mean (Appendix I) are consistent with previous results for the Permian–Triassic South China block (Yang and Besse, 2001), suggesting that the paleomagnetic directions from Shangsi that passed the selection criteria for inclusion are reliable, and consistent with the sediment remanence representing a primary magnetization acquired during or soon after deposition.

3.5. Magnetostratigraphy

Magnetostratigraphic results from parallel sections are in general agreement (Fig. 4), and mostly confirm the principal magnetozones of Heller et al. (1988). Some differences between our

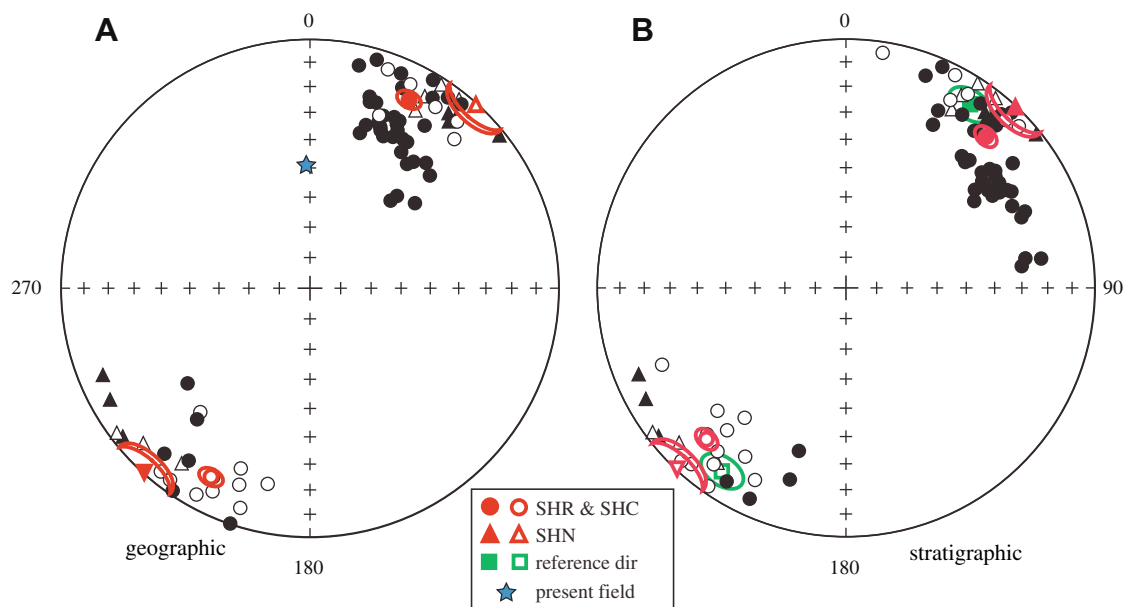


Fig. 3. (A) Stereonet showing sample directions (black) and section means (red) for the northwest-limb section (SHN, triangles) and combined southern sections (SHR and SHC, circles), before applying bedding corrections and, (B) after applying bedding corrections. Also shown are the present field direction (star) and the normal and reversed reference directions (squares) with their associated 95% confidence limits for the South China block (Yang and Besse, 2001). Open symbols are on the upper hemisphere. (For interpretation of the references in colour in this figure legend, the reader is referred to the web version of this article.)

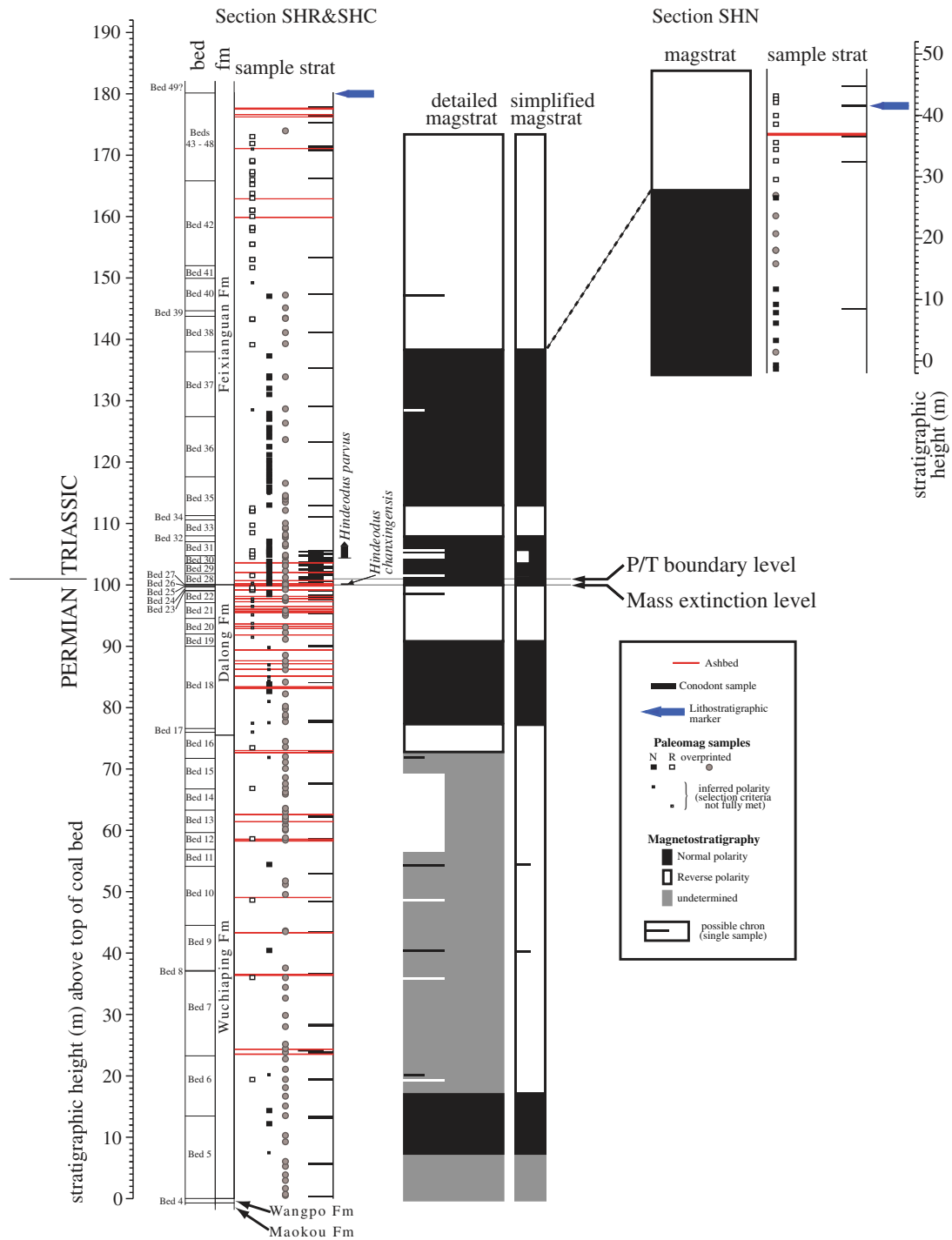


Fig. 4. Magnetostratigraphy of the Shangsi sections and their interpreted correlation. Lithostratigraphic markers (blue arrows) and magnetostratigraphy are used to correlate sections. A possible polarity chron, defined by a single sample, is shown by a bar that partially extends across the magnetostratigraphic column.

results and those of Steiner et al's. 1989 and Heller et al's. (1988) may be ascribed to the differences in the treatment of samples performed in the various studies, the effects of incomplete removal of overprints, and some ambiguities in correlating sample positions. A general agreement of the various studies, however seems to indicate that the magnetostratigraphy for the most part, is reliably reproduced within the section (Fig. 5). Given this general consistency, we believe that the data selection criteria effectively exclude low-stability magnetizations and strong secondary overprints, and that secondary overprints associated with the

remaining samples do not significantly limit our ability to determine their polarity.

The magnetostratigraphic correlation of the two nearby, parallel (southern) sections was corroborated by tracing stratigraphic units between sections. Correlating these with the third (northern) section located several miles away was more difficult due to the lack of exposure of the PT boundary in that section. Based on the general character of lithologic units, and on an estimate of the stratigraphic distance to the basal coal bed, which was exposed in a nearby mine, we correlated the normal-to-reversed polarity

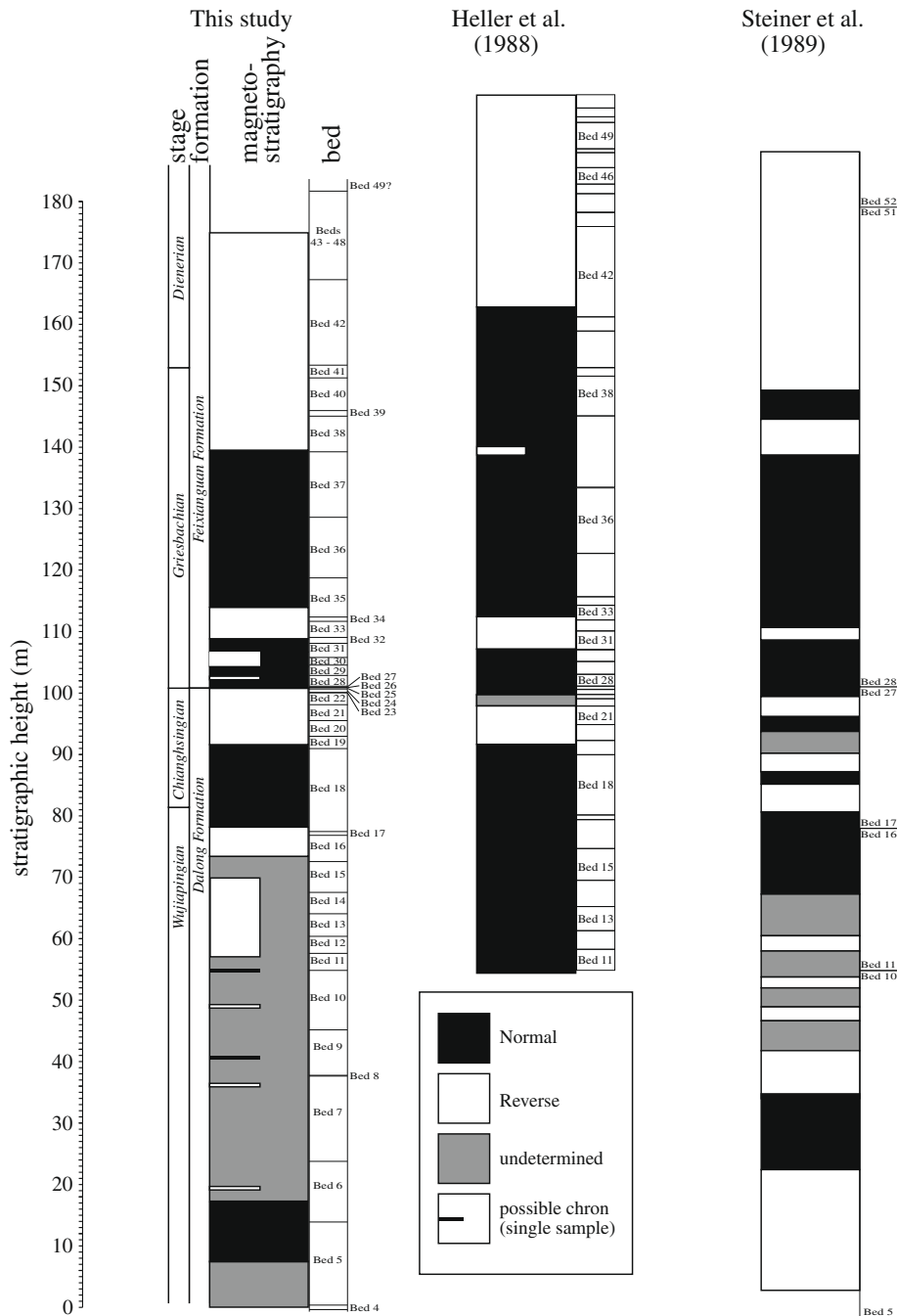


Fig. 5. Correlation of the composite Shangsi magnetostratigraphy (this study) with the two existing Shangsi studies of Heller et al. (1988) and Steiner et al. (1989).

transition in this section with that in the uppermost part of the main section (Fig. 4). This correlation is consistent with the limited biostratigraphic control that was recovered from high in the sequence from both southern and northern sections, where sufficient numbers of conodonts of the species of *Isarcicella* [samples 44 (112.5 m) and 47 (129 m) in the main southern section, and sample SHN/C-1 (22 m) in the northern section] confirm that the entire sampled sequence from the northern section lies above the biostratigraphic boundary.

The composite section spans a sequence of at least eight principal polarity chrons (Fig. 4) and shows that the onset of the Illawarra mixed interval lies below the measured section (which extends 50 m below the previous study of Heller et al., 1988) indicating that the uppermost Permian Changhsingian and at least part

of the Wuchiapingian stages postdate the end of the PCRS. Furthermore, given the new age data from Shangsi (Mundil et al., 2004), it can be concluded that the age of the Illawarra reversal marking the end of the PCRS is older than 260 Ma.

As mentioned above, the PT biostratigraphic boundary occurs within a normal polarity chron, 5 m above the inferred mass extinction level at the base of the clastic zone. Results from hand samples taken from the clastic zone lying immediately above the mass-extinction boundary indicate that at Shangsi, the onset of an R-N polarity transition is indistinguishable (within 50 cm) from the bio- and litho-stratigraphic boundary. This coincidence of magneto- and bio-stratigraphic boundaries will likely play a key role in interpreting how terrestrial and marine sections correlate.

4. Langdai sections, Guizhou Province

Near Langdai (NW Guizhou Province in the South China block), terrestrial to shallow marine (paralic) mudstone and carbonate sediments that span the PT boundary were sampled in two sections situated on opposing limbs of an anticline, located ~10 km apart. We sampled in detail near the inferred PT boundary at the Langdai sections to identify the R–N polarity transition found at or near the PT boundary in several marine sections (e.g., Heller et al., 1995, Fig. 1). High-resolution isotopic dating on ash layers, as well as biostratigraphic investigations in this section, are also being undertaken to aid correlations between the sections and to help constrain the timing of the PT biotic crisis.

4.1. Geologic setting

The Permian–Triassic Langdai sediments comprise a sequence of paralic sediments that outcrop near Langdai in northwest Guizhou Province in the South China block (Figs. 1 and 6). These sediments were subsequently folded probably sometime in the Jurassic (Yang and Besse, 2001).

The sediments from the Langdai sections consist of interbedded green, tan, grey, and brown sandstones, siltstones, mudstones and shales. In the Guizhou area, the upper Permian and lower Triassic belong to the Xuanwei Formation, which is overlain by the

Lower Triassic Kayitou Formation. For a detailed paleogeographic and stratigraphic description of the PT sections in the Guizhou province, see Peng et al. (2005).

Two sections were sampled (involving over 100 oriented cores, in total) to provide a fold test and duplicate magnetostratigraphies. The first section, at Zhongzhai, is located ~7.5 km northwest of Langdai within the northeast limb of a northwest-trending anticline with dips on the order of 20–30°. For detailed stratigraphic logs of the Zhongzhai section, see Metcalfe and Nicoll (2007). The second section, at Tanghaishui, located ~3.5 km west-southwest of Langdai and ~7 km south-southeast of Zhongzhai, occurs within the northwest limb of a second northwest-trending anticline displaying dips of 40–50°. The PT boundary is present in the Zhongzhai section but not at Tanghaishui. The two sections are correlated by bio- and litho-stratigraphy.

4.2. Biostratigraphy

Macrofaunal, palynoflora, and conodont faunas from the Langdai sections indicate the PT boundary lies between two sampled volcanic ash/clay layers (Metcalfe and Nicoll, 2007; Peng et al., 2005) at 6.23 and 6.38 m from the base of the measured section at Zhongzhai (Fig. 8). The PT boundary is unequivocally determined as occurring between these two ash beds by two conodont faunas in limestone beds immediately below and above which contain

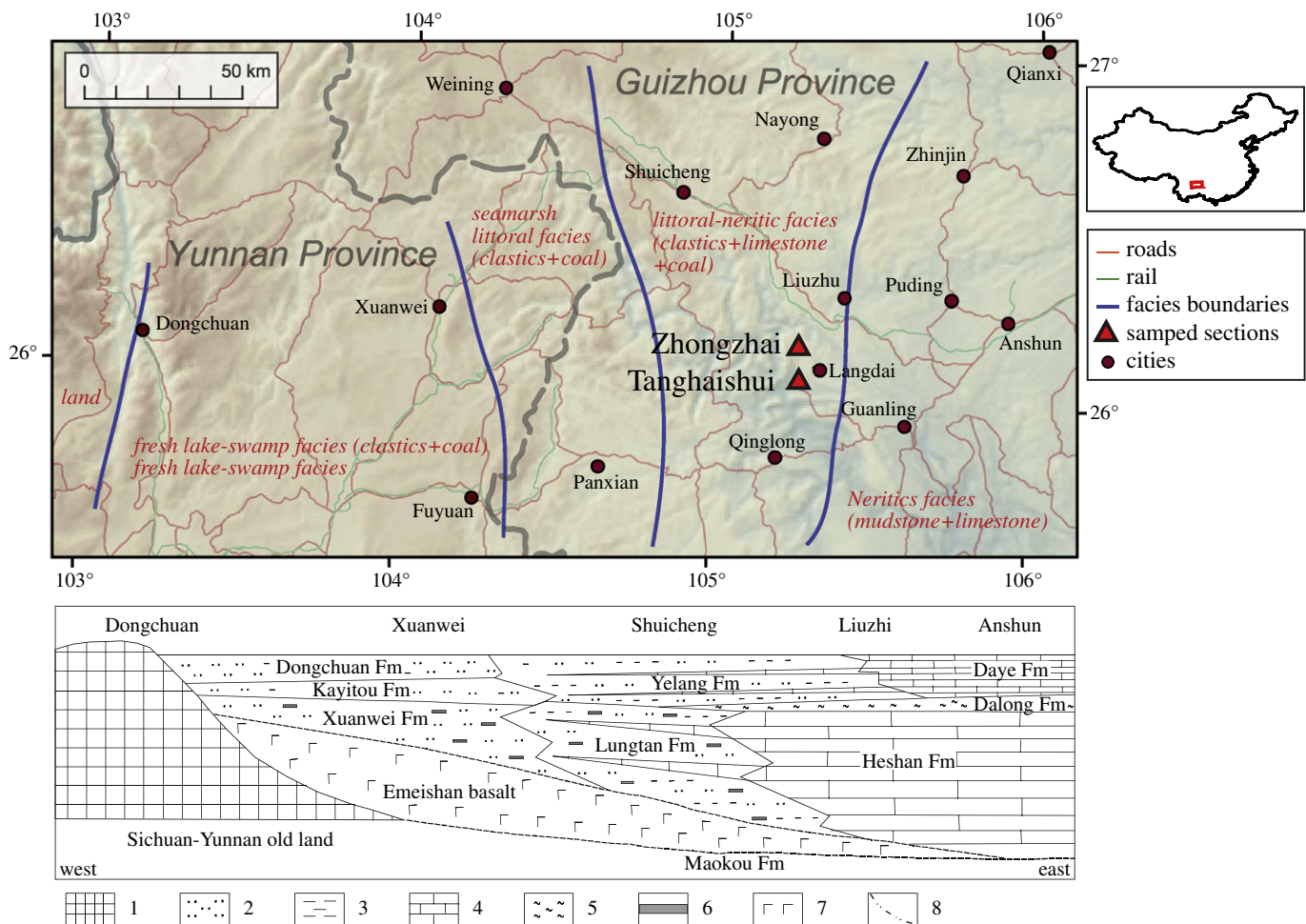


Fig. 6. Index map showing the location of sampled Langdai sections (Zhongzhai and Tanghaishui), Guizhou Province. Also shown are transportation routes (black lines), province boundaries (dashed grey line), and facies boundaries (blue lines). Lower panel shows the generalized paleogeography and lithostratigraphy of the displayed region. Units include: (1) landmass; (2) sandstone and/or siltstone; (3) mudstone and/or shale; (4) limestone; (5) chert; (6) coal; (7) basalt; (8) facies boundary. Modified from Peng et al. (2005). (For interpretation of the references in colour in this figure legend, the reader is referred to the web version of this article.)

typical latest Changhsingian and basal Triassic (with *H. parvus*) conodonts. The mass extinction level is placed at the top of a 50 cm thin dark grey shale with Changhsingian brachiopods and the R–N polarity transition determined here occurs within this mudstone (Metcalf and Nicoll, 2007).

4.3. Rock magnetic results

Both Langdai sections yield similar rock magnetic characteristics. The majority of samples, regardless of their individual lithology, have a magnetic mineralogy dominated by titanium-poor titanomagnetite with minor ilmenohematite. Average NRM intensities and magnetic susceptibilities were 1.5×10^{-1} A/m, and 6.6×10^{-3} SI units, respectively. Thermomagnetic susceptibility (K–T) curves, for the majority of samples, generally show a steep drop in susceptibility around 550 °C to 580 °C (Appendix A2). We interpret the steep drop as the Curie temperature of low-Ti titanomagnetite, while the persistence of some susceptibility above 600 °C suggests the presence in some cases of ilmenohematite. AF demagnetization to 100 mT did not completely demagnetize these samples, further suggesting the presence of a high coercivity component such as ilmenohematite and/or goethite. Reflected light microscope observations reveal detrital magnetite grains, with ilmenite lamellae exsolutions, that range in size from 1 to 45 μm .

The rock magnetic results (Appendix A1) and petrological observations discussed above suggest that titanomagnetite, the most likely primary carrier of magnetization in these types of sediments, dominates the sample remanences such that these samples should be good paleomagnetic recorders. The remanence data are consistent with this conclusion, as most of the samples from these sediments yield stable endpoint magnetizations or stable two-component great-circle magnetizations. The presence of ilmenohematite and goethite is of concern, as it probably carries a secondary remanence, but the majority of data presented below indicate that the effects of this component on our polarity determinations are minor. Large increases in susceptibility observed in some K–T curves upon cooling from 700 °C (Appendix A2, C and F) as well as ‘bumps’ in curves upon heating, in the range of 300–400 °C (Appendix A2, A and D), suggest the presence and alteration of iron sulfides.

4.4. Magnetic remanence results

In order to determine the magnetic stratigraphy, we measured and stepwise AF and thermally demagnetized 83 samples from the two Langdai sections. Natural remanent magnetization directions from all sections cluster around the PDF direction in geographic coordinates (Appendix C2) and scatter after bedding correction, indicating that the NRM directions reflect a post-folding PDF overprint.

Thermal demagnetization was the most effective technique for removing overprints (Appendices D2, E2). A presumably viscous, PDF overprint of north and down disappeared between 150 °C and 400 °C (typically below 250 °C). A high stability component that decayed linearly toward the origin was revealed in nearly 80% of the samples. These characteristic remanent components were typically isolated between 450 °C and 600 °C. The stable endpoint directions determined from the demagnetization data appear to be primary PT directions, as the mean section directions (Fig. 7) pass a fold test.

Roughly 20% of all samples were seriously effected by strong, unremoved overprints. All reversed directions in the Zhongzhai section were obtained using great circle analysis (Appendix F2). In general, these great circle magnetizations were stable over a temperature range similar to that for which characteristic directions were isolated in samples yielding stable endpoint magnetizations (450–500 °C) though, in some cases above 450 °C to 500 °C, magnetizations became unstable or trended toward anomalous directions. Applying the data selection criteria discussed earlier, we accepted polarity determinations from 84% of the 83 samples measured. For a summary of the accepted data, see Appendix G2.

Section-mean directions pass a fold test at the 95% confidence level, and normal and reversed directions are roughly antipodal. Furthermore, the Langdai locality mean direction lies close to the reference PT direction of Yang and Besse (2001). We consider these results to indicate that the Langdai data reflect reliable pre-folding primary PT magnetizations.

4.5. Magnetostratigraphy

Sample polarities were determined from these data to yield section magnetostratigraphies listed in Appendix G2 and shown in

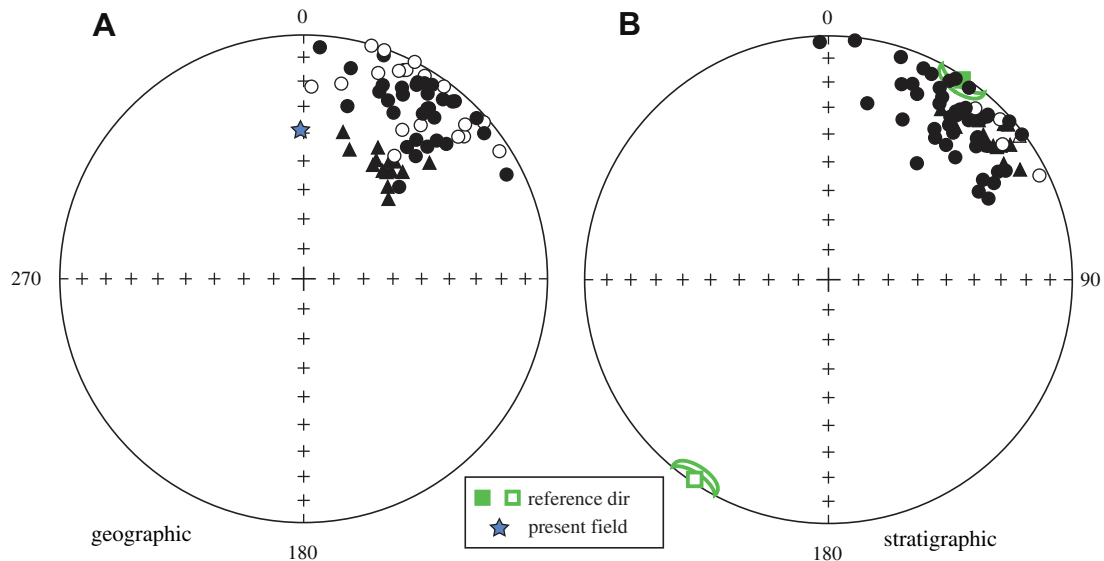


Fig. 7. Stereonets showing the Langdai sample directions of magnetization before (A) and after (B) applying bedding corrections. Also shown are the present field direction (star) and the reference direction (square) with its associated 95% confidence limit for the South China block (Yang and Besse, 2001). Open symbols are on the upper hemisphere.

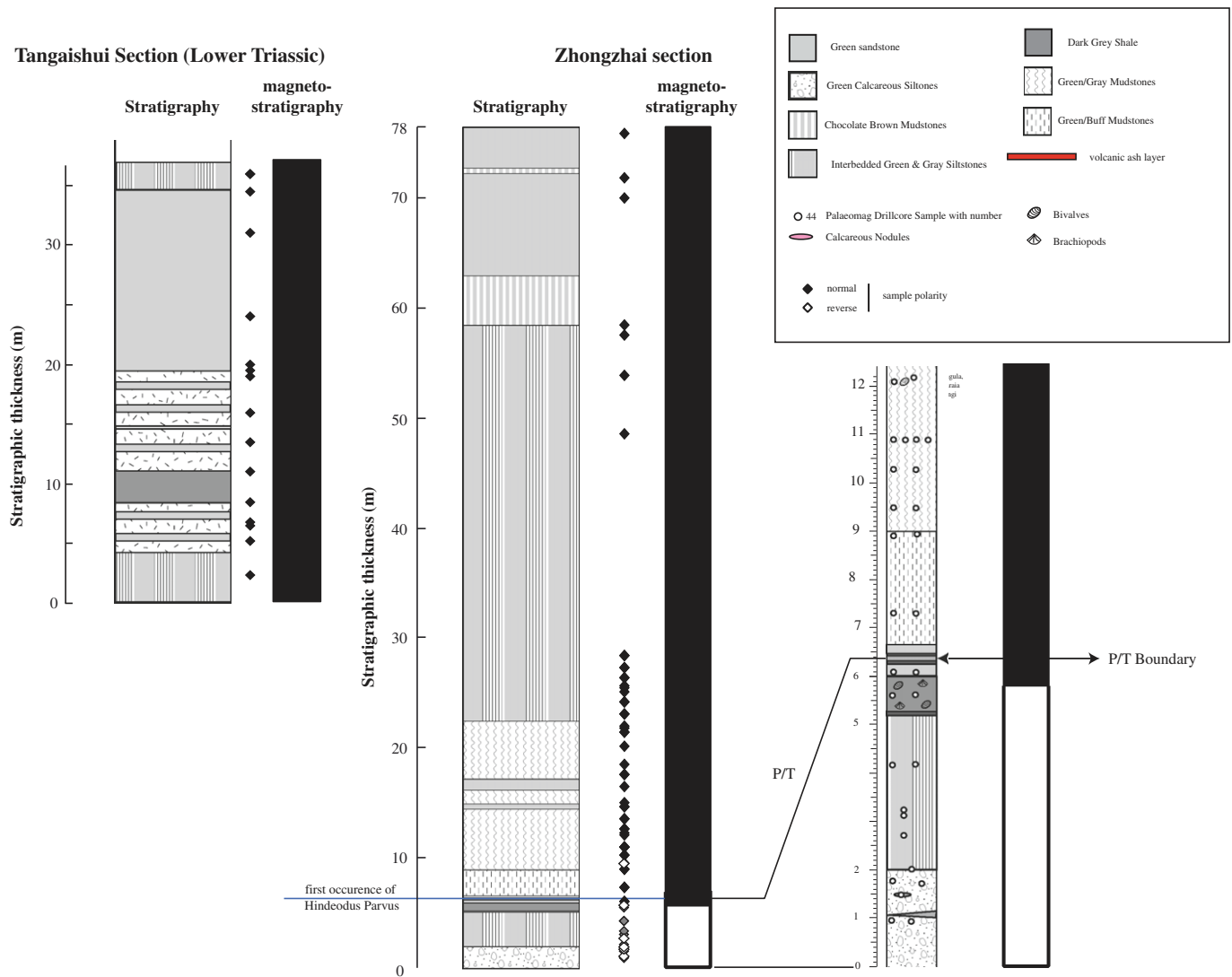


Fig. 8. Magnetostratigraphy and correlation of the Langdai sections. Shown is the sample polarity determined from best-fit sample directions or from demagnetization great circle trends, and interpreted magnetostratigraphy.

Fig. 8. The magnetostratigraphies of the two sections are consistent with the biostratigraphic correlation and with reasonable estimates of expected deposition rates. The two section magnetostratigraphies are consistent and result in the composite magnetostratigraphy shown in Fig. 8. The composite section spans an R-N polarity sequence.

5. Junggar terrestrial, Xinjiang Province

Lacustrine-fluviatile sedimentary sections from the southern Junggar Basin in the northern Bogda Shan foothills of Xinjiang Province, NW China, are believed to represent some of the best exposed and most complete PT-boundary terrestrial sequences in the world. We have sampled three duplicate sections for magnetostratigraphy believed to span the non-marine sequence of the Cangfanguo group from the late Permian to early Triassic. Two of the sections were taken from opposing limbs of an anticline, while the third was sampled some 100 km away.

The focus of this study was to locate the end of the nearest sizeable reversed chronozone to the inferred biostratigraphic boundary of Ouyang and Norris (1999). This R-N polarity transition has

been found at or near the PT boundary in several marine and continental sections (e.g., Gallet et al., 2000; Nawrocki, 2004; Szurlies et al., 2003) and, in combination with a good biostratigraphy of the section, could provide a robust correlation of this sequence to the marine sequence.

5.1. Geologic setting

The Cangfanguo group is a sequence of lacustrine to fluvial sediments that outcrop along the southern margin of the Junggar basin (Figs. 1 and 9). These sediments supposedly accumulated in and around a large lake that covered much of the ancestral basin (Carroll, 1998); they were subsequently folded and exposed during the most recent stage (roughly 5 Ma) of uplift along the Tien Shan (Avouac et al., 1993). Ouyang and Norris (1999), argue that sedimentation of this group was continuous through the PT boundary. Based on a combination of their own palynologic data and the paleontologic data of Li et al. (1986a), they placed the PT biostratigraphic boundary within the Guodikeng Formation, thirty meters below the Guodikeng-Juicaiyuan lithologic boundary. Previous paleomagnetic studies of the Cangfanguo group include two tectonic studies (Nie et al., 1993; Sharps et al., 1992) and one magnetostratigraphic study

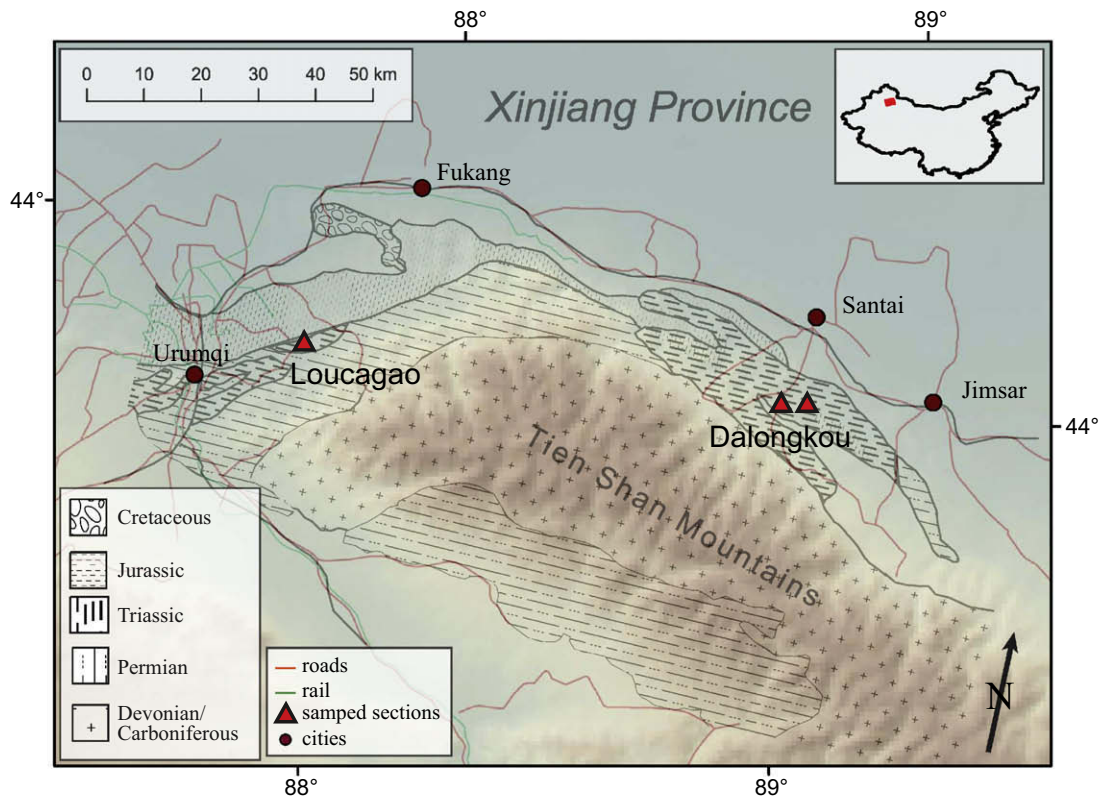


Fig. 9. Index map showing location of sampled Junggar sections (Lucaogou and Dalongkou) in the southern Junggar basin, Xinjiang Province (modified from Ouyang and Norris, 1999).

(Li et al., 1981), none of which have the stratigraphic resolution necessary for the precise correlation that we seek.

Three sections of this sequence were sampled for this study. The first two sections (Dalongkou North and Dalongkou South) were on the north and south limbs of the steeply dipping Dalongkou anticline, 20 km west of Jimsar (Fig. 9). The third section, Lucaogou, was taken in an overturned monocline located 20 km east of Urumqi (Fig. 9). We loosely correlated the three sections based on a few sharp lithologic boundaries. Dips of the beds were steep to overturned: Dalongkou north limb attitudes varied between 70° and 83° to the north, Dalongkou south limb attitudes varied between 55° and 125° to the south, and Lucaogou attitudes were all roughly 115° to the northwest.

Sampling for the present study spanned the lower Wutonggou Formation, through the overlying Guodikeng Formation, and into the lower Jiucaiyuan Formation. Lithologically, the late Permian (P_2) Wutonggou Formation comprises several thick beds of fine to medium-grained tan sandstones with brown mudstone interbeds. The transitional ($P_2 - T_1$) Guodikeng Formation comprises friable brown laminated mudstones and small intervals of green, grey, tan, and purple sandstones, siltstones, and shales. The Jiucaiyuan Formation, where sampled, is characterized by thick beds of light colored sandstones interbedded with brown mudstones. For a more detailed stratigraphic description of these sections, see Metcalfe et al. (this issue).

5.2. Biostratigraphy

The placement of the PT boundary at Dalongkou and Lucaogou on biostratigraphic criteria is equivocal. However, available biostratigraphic, chemostratigraphic and palaeoclimatic data (see Metcalfe et al., this issue) suggests that the PT boundary is located

high in the Guodikeng Formation or even as high as the basal Jiucaiyuan Formation at Dalongkou. An overlap of the Upper Permian *Dicynodon* and Lower Triassic *Lystrosaurus* vertebrate fossil assemblages suggests the boundary is at or higher than the last appearance datum (LAD) of *Dicynodon* (at ~180 m above the base of the Guodikeng Formation) in the uppermost Guodikeng. This placement is supported by conchstracan biostratigraphy (Metcalfe et al., this issue).

As part of a companion study, palynomorphs have also been studied. Samples from this study yielded far more palynomorphs than any previous study and three palynomorph assemblages have been recognized (Metcalfe et al., this issue). The upper assemblage, characterized by *Lundbladispora foveata*, *Pechorosporites disertus* and *Otynisporites eotriassicus* includes both typical Permian and Triassic forms and a high proportion of abnormal pollen grains indicative of severe climatic conditions (Foster and Afonin, 2005). It is interesting to note that despite high palynomorph yields and large numbers of samples, the key Early Triassic form *Aratrisporites* was not recovered suggesting that earlier accounts (Ouyang and Norris, 1999), which indicate its presence in the upper Guodikeng Formation, may not be reliable. Furthermore, while *Otynisporites* mostly occurs in the uppermost Permian, and is generally restricted to the latest Permian, it has been found (Greenland, Wordie Creek Formation, Jameson Land – Foster and Afonin, 2005) several meters above the first appearance of *Hindeodus parvus* in the Lower Triassic. Their occurrence, therefore, does not necessarily indicate a Permian age. Palynomorphs therefore do not allow for an accurate placement of the mass extinction level in the sections at present (Foster et al., 2002). In summary, the PT boundary lies – conservatively reckoned – somewhere in the uppermost part of the Guodikeng Formation, or lower part of the overlying Jiucaiyuan Formation.

5.3. Rock magnetic results

Data from all of the Junggar sections indicate the presence of titanomagnetite, though distinct differences between the formations was evident in IRM acquisition curves, Lowrie experiments, and certain K–T curves (Appendices A3, B2). Average NRMs were 1.03×10^{-1} A/m, 3.29×10^{-2} A/m, and 1.2×10^{-2} A/m for Guodikeng, Jiucaiyuan, and Wutonggou formations, respectively. Average initial susceptibilities were 2.8×10^{-3} SI, 7.1×10^{-4} SI, and 6.9×10^{-4} SI for the Guodikeng, Jiucaiyuan, and Wutonggou formations, respectively.

The majority of samples from the Guodikeng and Jiucaiyuan formations have a magnetic mineralogy dominated by Ti-poor titanomagnetite with minor ilmenohematite and less common titanomaghemite. Thermomagnetic susceptibility (K–T) curves generally show a steep drop in susceptibility between 520 °C and 580 °C, followed by a small tail of susceptibility up to 680 °C (Appendix A3). We interpret the steep drop as reflecting the Curie temperature of low-Ti titanomagnetite. However, the persistence of some sample remanence above thermal demagnetization to 600 °C and above AF demagnetization to 200 mT, as well as ferromagnetic susceptibility up to 680 °C, suggests the presence of ilmenohematite. A few samples from the Guodikeng Formation (not shown) display a small irreversible bulge in susceptibility between 150 °C and 450 °C that probably indicates titanomaghemite that inverted during heating. Data from IRM acquisition experiments corroborate the dominance of titanomagnetite and presence of ilmenohematite; sample magnetizations reach substantial saturation at low applied fields (0.1 T, Appendix B2), followed by small increases in magnetization at higher fields. Data from 3-axis IRM thermal demagnetization experiments (Appendix B3) show a low-coercivity, high intensity magnetization that is largely destroyed by 550 °C (probably titanomagnetite) and a high coercivity, low intensity magnetization that persists up to higher temperatures (probably ilmenohematite).

The rock magnetic results discussed above suggest that titanomagnetite, the most likely primary carrier of magnetization in

these types of sediments, dominates the sample remanences such that these samples should be good paleomagnetic recorders. The remanence data are consistent with this conclusion, as most of the samples from these formations yield stable endpoint magnetizations or stable two-component great-circle magnetizations. The presence of ilmenohematite is of concern, as it probably carries a secondary remanence, but the majority of data presented below indicate that the effects of this component on the polarity determinations are minor.

Wutonggou samples showed unusual K–T behavior (Appendix A3, E and F) that was not observed in either Guodikeng or Jiucaiyuan samples. Their K–T curves are mostly flat up to between 425 °C and 500 °C, above which the majority of the data show a spike in susceptibility that drops sharply back down at an average temperature of 550 °C, later followed by large increases in susceptibility on cooling. This spike indicates chemical reactions upon heating that likely reflect the creation of magnetite from a very weakly magnetic or paramagnetic iron phase. Some sample data lack the K–T reaction spike but nonetheless show the strong gain in susceptibility on cooling, indicating that the same reaction occurred, only more slowly or at a higher temperature. IRM acquisition experiments further suggest that magnetite was generated by this reaction: these samples show similarly shaped IRM acquisition curves before and after heating to 550 °C, but with substantial increases in saturation magnetization after heating.

The oxidation of pyrite to magnetite is the best explanation for this K–T behavior because this reaction occurs over a temperature range comparable to that observed in other experiments and because pyrite is paramagnetic, explaining why we see no magnetic evidence for this phase until it oxidizes. Examination of selected samples under reflected light and analysis by an ARL scanning electron microscope quantometer revealed <50 μm high reflectance grains of pyrite as well as larger grains of rutile, ilmenite, and titanomagnetite. The presence of pyrite in this formation is unusual given the oxic nature of the depositional environment, but we are unable to speculate on whether this pyrite is detrital, diagenetic, or secondary (Machel, 1996). Regardless of how it arrived in

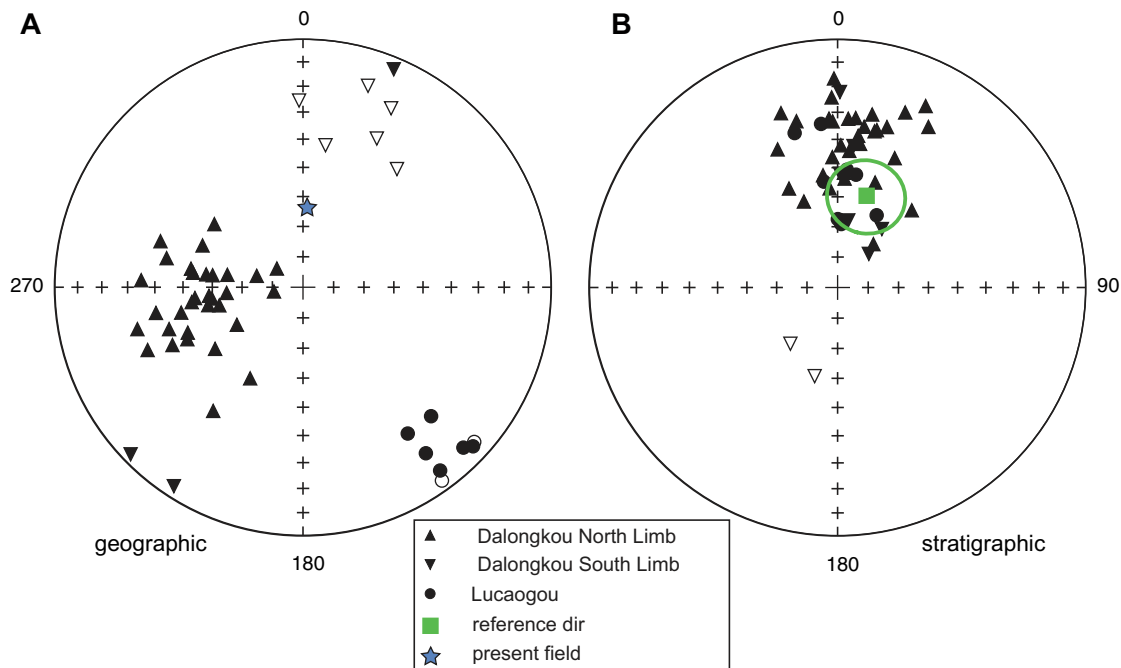


Fig. 10. Stereonets showing the Junggar sample directions of magnetization (A) before, and (B) after applying bedding corrections. Also shown are the present field direction (star) and the normal and the reversed reference directions (square) with its associated 95% confidence limit for the Junggar Basin (Nie et al., 1993). Open symbols are on the upper hemisphere.

the sediments, the presence of paramagnetic pyrite could have no effect on the primary magnetization of the samples.

As with the Jiucuiyuan Formation, we were able to determine polarities from many of these samples, although there was a greater proportion of unstable or completely overprinted samples from the Wutonggou Formation than from the Guodikeng Formation. The weaker magnetic properties of the Wutonggou samples, in combination with the disruption caused by the pyrite-magnetite reaction, may explain the lower quality remanence data.

5.4. Magnetic remanence results

In order to determine the magnetic stratigraphy, we stepwise AF and thermally demagnetized over 300 samples from the three sections. Natural remanent magnetization directions from all sections cluster around the PDF direction in geographic coordinates and scatter after applying bedding corrections (Appendix C3), indicating that the NRM directions are consistent with a post-folding PDF overprint.

Thermal demagnetization was the most effective technique for removing strong PDF overprints and for revealing high-stability secondary overprints. Thermal demagnetization completely removed the PDF overprint and isolated a linear high stability component in 16% of the samples, almost all of which came from the Guodikeng Formation. In these data, a presumably viscous overprint of north and down disappeared by between 250 °C and 400 °C, after which sample magnetizations of both polarities decayed linearly toward the origin (Appendix D3) up to between 450 °C and 600 °C. Above 500 °C to 600 °C, these magnetizations usually became unstable or trended toward anomalous directions (Appendix E3).

Lowrie experiment data from these samples suggest that the demagnetization behavior (Appendices B2, D3) is the result of the demagnetization of a dominant titanomagnetite component up to around 500 °C, followed by the dominance of a high stability ilmenohematite component to above 600 °C. Below 550 °C, directional data from these tests (not shown) reveal that the composite magnetization direction of these artificially magnetized samples remained close to the direction of the softest IRM axis that should be carried primarily by titanomagnetite. We therefore limit our interpretation of the sample demagnetization data to the range in which the effects of the ilmenohematite are minimized (below 550 °C).

Due to strong overprinting by the present day field, nearly all sample magnetizations from the Jiucuiyuan and Wutonggou formations and many sample magnetizations from the Guodikeng Formation did not attain stable endpoints. The majority of these less ideal data did, however, trend along stable great circles that trend between the PDF overprint direction and a ChRM that is quite consistent with the stable endpoint directions discussed above (Appendix E3). In general, these great circle magnetizations were stable over a temperature range similar to those magnetizations that attained stable endpoints (100–500 °C), and they trend from the PDF direction (Appendix F3) toward roughly the same direction that was attained by the stable endpoint magnetizations discussed above (Fig. 10). In the Guodikeng Formation, rock magnetic data from the samples with great circle magnetizations are indistinguishable from rock magnetic data of those with stable endpoint magnetizations, so we cannot attribute the tenacity of the PDF overprint to any difference in rock properties.

We discarded samples with unstable demagnetization, significant PDF overprints, and strong secondary high-stability overprints. Based on the criteria discussed above, we accepted and determined polarity from 201 of the 314 samples measured. For a summary of the accepted data, see Appendix G3.

Although these stable endpoint directions (Fig. 10), as well as the locality mean (Appendix I), lie near the expected direction of Nie et al. (1993), they yield reversal and fold tests that are inconclusive. This is likely due to unremoved secondary syn- or post-folding magnetizations (e.g., carried by ilmenohematite). The persistence of secondary components, which may limit our ability to determine an accurate PT paleomagnetic pole, nonetheless, is not considered to have significantly undermined our ability to determine sample polarity.

5.5. Magnetostratigraphy

Applying the data selection criteria, we obtained the results listed in Appendix G3 and shown in Fig. 11. It is notable that the

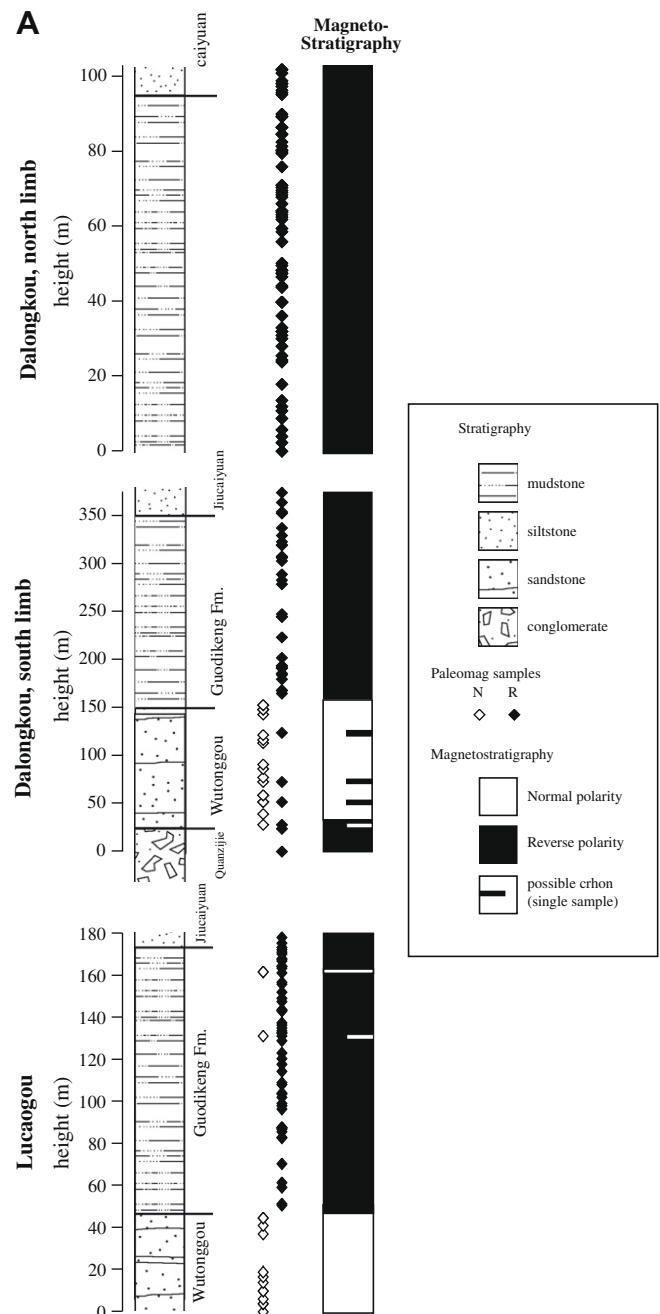


Fig. 11. Magnetostratigraphy of the Junggar sections and their interpreted correlation. (A) lithostratigraphy, sample position and polarity, and magnetic stratigraphy. (B) Correlation of the three sections and their composite magnetostratigraphy.

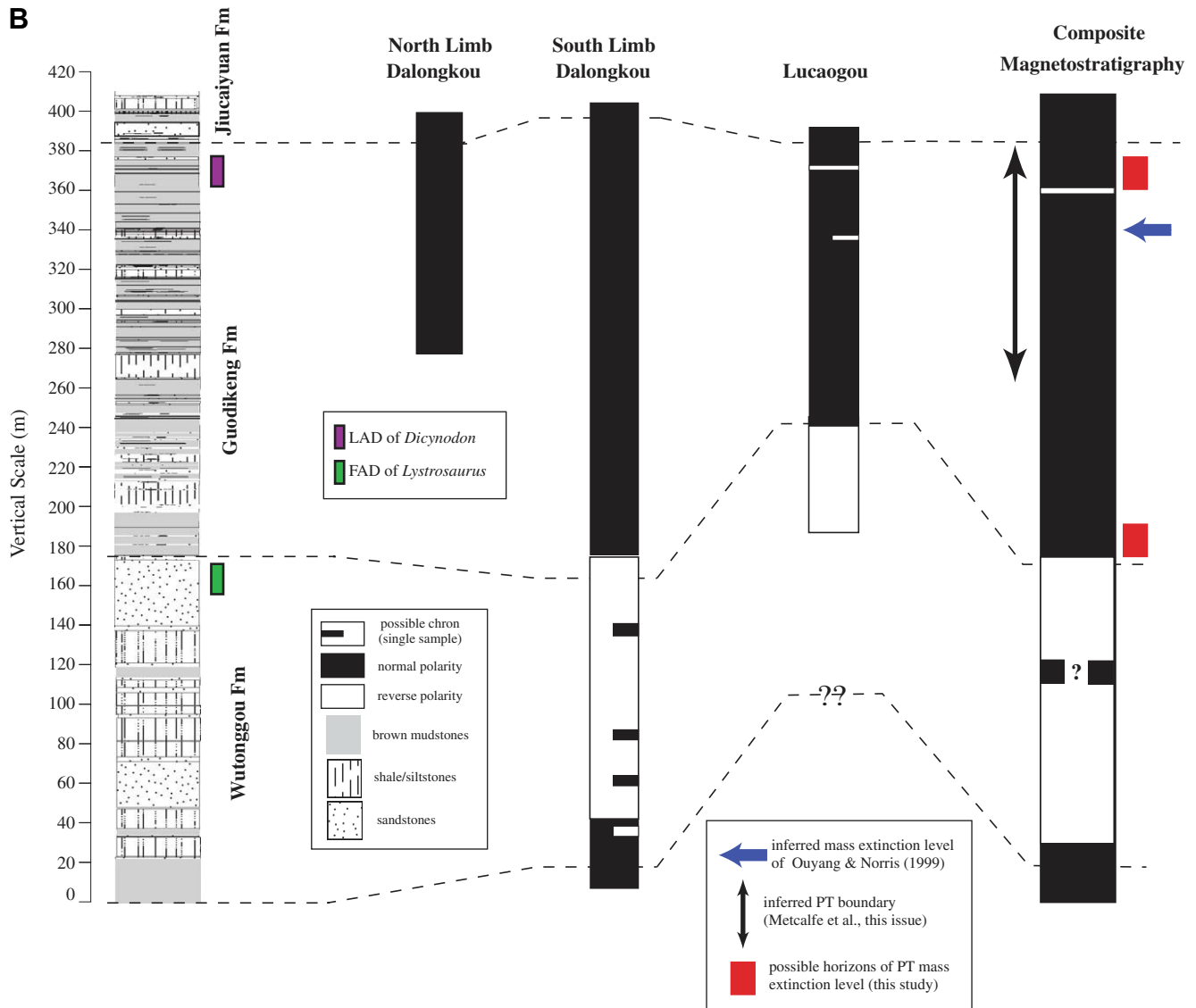


Fig 11. (continued)

polarity results shown for all of the sections do not change if we include those samples that we excluded based on the criteria discussed above. Nonetheless, we cannot fully account for nor remove the overprints; we therefore chose to exclude these data from our final results.

We consider these results to yield a reliable PT magnetostratigraphy because both polarities are present and are roughly antipodal, and because our directions agree with previous late Permian results from the Junggar basin. More importantly, the three magnetostratigraphies appear highly consistent; if a remagnetization had occurred, it must have occurred at very consistent stratigraphic levels across a lateral distance of 100 km.

The composite Junggar magnetostratigraphy is shown in Fig. 11. The small reversed chronozone seen in the Guodikeng Formation at Lucaogou is missing at Dalongkou, likely due to that fact that the chronozone is sufficiently thin (<1.5 m) such that we could have missed sampling it in the Dalongkou sections. In the Dalongkou south limb and Lucaogou sections, there is a slight disagreement in the location of the major R-N polarity transition; the transition is just above the Wutonggou/Guodikeng lithologic boundary at Dalongkou, whereas it occurs at the lithologic boundary at Lucaogou. We attribute this discrepancy to the lack of suit-

able samples in the 10 m above the lithologic boundary at Lucaogou. The reversed chron at Lucaogou may continue several meters into the lower Guodikeng, but we were unable to sample those rocks due to lack of exposure.

A persistent feature of the marine PT magnetic record is an R-N polarity transition at or just above the end-Permian mass extinction level. The closest R-N transition in the $P_2 - T_1$ formations of the Canfanggou group is just above the Wutonggou–Guodikeng formation boundary, surprisingly over 160 m below the inferred biostratigraphic boundary of Ouyang and Norris (1999). Although there is a short reversed chron in the upper Guodikeng Formation, it seems unlikely, based on generally accepted sedimentation rates, that this <1.5 m thick chron in a non-marine section is the equivalent of the ~5–10 m thick reversed chrons seen below the PT boundary in the marine and paralic sections. Also, because we sampled the Guodikeng Formation at the three sections in detail and because the Guodikeng samples yielded good quality data, it is unlikely that we missed a large reversed chron in that formation. Rather, our magnetostratigraphic correlation of the Junggar sections to Chinese marine sections suggests that there is a sizable mismatch between the marine biostratigraphic boundary and the non-marine mass extinction boundary placement of Ouyang and

Norris (1999) at the Junggar sections. As noted earlier, there is reason to question the placement of the boundary by Ouyang and Norris (1999). Thus, assuming that the marine magnetostratigraphies are correct and that the PT biostratigraphic transition was even remotely time-equivalent in the marine and non-marine realms, the simplest interpretation of our data is that the mass extinction boundary has been misplaced in these sections.

On biostratigraphic grounds (see above), the PT boundary is best positioned somewhere between the middle Guodikeng Formation and the lowest Jiucuiyuan Formation. In light of this, the mass extinction level may correspond with a short reversed chron in the upper Guodikeng Formation, consistent with the interpretation of Ouyang and Norris (1999), or with the R-N polarity reversal near the Wutonggou–Guodikeng formation boundary. In the former case, the upper Guodikeng Formation must be highly condensed, characterized by significantly lower sedimentation rates or containing hiatuses. We consider the latter case to be more likely as it does not require large stratigraphic gaps or fluctuations in deposition. In addition, this interpretation is consistent with records from South Africa (De Kock and Kirschvink, 2004; Ward et al., 2005) that indicate the R-N reversal falls within an overlapping interval of co-occurrence of *Lystrosaurus* and *Dicynodon*, and that the lowest occurrence of *Lystrosaurus* lies in an interval of reversed polarity.

6. Discussion

Paleomagnetic data from the three studied localities at Shangsi, Langdai, and Junggar yield consistent results from parallel, overlapping sections, and provide locality means that lie close to their respective PT and Lower Triassic reference poles, suggesting that the paleomagnetic directions are consistent with the sediment remanence representing primary PT magnetizations.

Magnetostratigraphic studies at Shangsi (Figs. 4 and 5), which indicate that the composite section contains at least eight principal polarity chrons, are consistent with other PT records (Fig. 12) that show the Late Permian to Early Triassic spanned several (5–10)

normal polarity chrons. The composite magnetostratigraphy from Shangsi, which bottoms out in a normal polarity chron, shows that the onset of the Illawarra mixed interval lies below the sampled section, indicating that the uppermost Permian Changhsingian and at least part of the Wuchiapingian stages postdate the end of the Permo-Carboniferous Reversed Superchron (PCRS). Because the Shangsi record did not extend to the Illawarra reversal that marks the end of the PCRS, we are unable to address the timing of its termination. As no reliable dates spanning the PCRS have been obtained from any of the existing studies, the age of this critically important marker for correlating Permian sections remains poorly-constrained but can be confidently placed at >260 Ma (as shown at Shangsi, Mundil et al., 2004).

Magnetostratigraphic studies at Shangsi reveal that the PT extinction level corresponds closely with an R-N polarity transition. Paleomagnetic results from hand samples taken from the clastic zone lying immediately above the mass-extinction boundary, indicate that at Shangsi, the onset of the R-N polarity transition is indistinguishable (within 50 cm) from the bio- litho-stratigraphic boundary. A number of other marine PT boundary sections from around the world (e.g., Gallet et al., 2000; Nawrocki, 2004; Szurlies et al., 2003) similarly show an R-N transition occurring at or near the PT boundary (Fig. 12). Paleomagnetic results from Langdai sections (Fig. 8) show that the combined paralic stratigraphy spans an R-N polarity sequence interpreted as the same R-N transition found to be coincident with the PT extinction level at Shangsi.

Magnetostratigraphic results from the Siberian Traps (Gurevitch et al., 1995), also indicate that the inferred PT boundary coincides with an R-N polarity chron boundary. In addition, recalculated ages from the Siberian traps (Min et al., 2000; Mundil et al., 2006b; Renne et al., 1995) based on data reported by Renne and Basu (1991) are indistinguishable from each other and from the accepted age of the PT boundary (Mundil et al., 2004) within uncertainties of perhaps 200 ka. These results indicate that the normal chron, spanning most of the Abaglakh–Noril’sk section (Gurevitch et al., 1995), likely corresponds with the normal chron in the Chinese sections reported here that extends across the PT

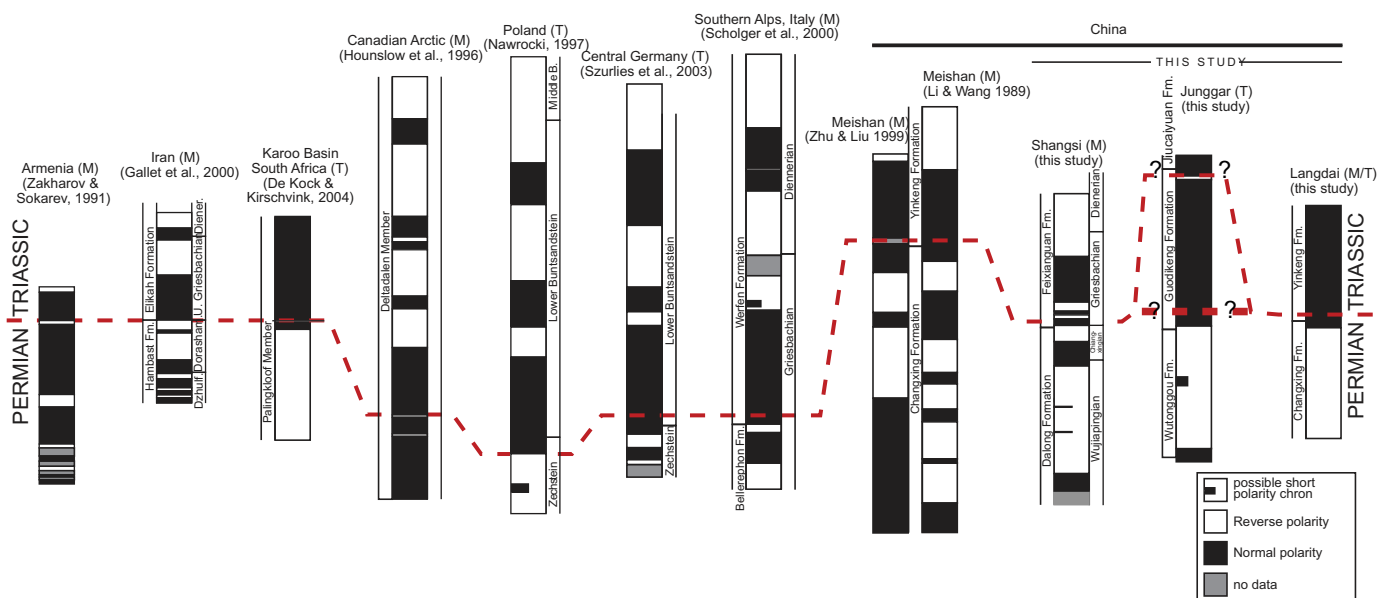


Fig. 12. Correlation of the composite section magnetostratigraphies of the Shangsi, Junggar, and Langdai localities with other PT marine records from around the world. Records shown include (from left to right): Armenia, Zakharov and Sokarev (1991); Iran, Gallet et al. (2000); South Africa, De Kock and Kirschvink (2004); Svalbard Arctic, Hounslow et al. (1996); Poland, Nawrocki (1997); Germany, Szurlies et al. (2003); Italy, Scholger et al. (2000); China (Meishan), Zhu and Liu (1999); China (Meishan), Li and Wang (1989); China (Shangsi), this study; China (Langdai), this study; China (Junggar), this study. Terrestrial (T), Marine (M) and paralic (M/T) sections are indicated.

boundary, consistent with claims that the bulk of the Siberian Traps were erupted in a relatively short period of time (perhaps on the order of 1 m.y. or less). Because the magnetic polarity reversal near the PT coincides with lithologic and presumed mass extinction boundaries, it provides a convenient proxy for identifying the PT and extinction levels in other (particularly terrestrial and non-marine) sections.

Paleomagnetic results from the southern Junggar basin (Fig. 11) yield a composite magnetostratigraphy containing three principal polarity chrons (N-R-N). The principal reversed chron recovered from the Junggar sections may correspond with the latest Permian reversed chron recorded in the Shangsi and Langdai sections. While this would indicate that the Guodikeng Formation represents a somewhat expanded section compared to the marine and paralic records, it is consistent with bio- and magneto-stratigraphic results from other terrestrial records (De Kock and Kirschvink, 2004; Ward et al., 2005). An alternative interpretation would be that the mass extinction level lies above a short reversed chron in the upper Guodikeng Formation, near the inferred boundary of Ouyang and Norris (1999). While we cannot preclude this possibility, it is not consistent with the results of De Kock and Kirschvink (De Kock and Kirschvink, 2004), and would imply the Guodikeng Formation is highly condensed compared to the rest of the composite Junggar section.

There was no opportunity to radio-isotopically date the Junggar sections, due to the lack of volcanic deposits there. Hence, the PT boundary cannot be placed unequivocally in the sampled Junggar sections. Thus we are precluded from addressing any potential phase-lag in the timing of terrestrial and marine responses to the end-Permian extinction event. However, the Langdai sections, allow for a comparison of paralic and marine environments. The Langdai sections, like those at Shangsi, show the inferred mass extinction level to closely correspond to the PT proximal R-N polarity transition (within 50 cm) and to be slightly lower than the first appearance of *H. parvus* (less than 1 m at Langdai and ~4.5 m at Shangsi). Therefore, to within the resolution of our sampling (~50 cm) there appears to be no lag in the timing of the inferred extinction boundary in marine and paralic sections.

7. Conclusions

We have studied three Chinese Permian–Triassic (PT) localities spanning terrestrial, paralic, and marine environments from localities at Junggar (Xinjiang Province), Langdai (Guizhou Province), and Shangsi (Sichuan Province), respectively. The primary focus of this work was to establish the magnetostratigraphy of the three study localities within the framework of radio-isotopic, chemostratigraphic, biostratigraphic and lithostratigraphic records to tie PT paralic, non-marine, and marine environments, and assess the timing of PT-boundary events on land and in the oceans. It was of particular interest to establish the precise occurrence of a reversed-to-normal (R-N) polarity transition, previously reported to lie approximately near the PT boundary at several PT marine sections, that could provide a key means of correlating the sections. To locate this polarity transition, we sampled in detail near the PT boundary so that we might be able to correlate the marine and non-marine sections at the meter or sub-meter scale.

At Shangsi our results confirm the polarity stratigraphy of Heller et al. (1988), while also providing magnetostratigraphy from parallel sections, and more detailed sampling. The composite magnetostratigraphic record shows that the onset of the Illawarra mixed interval lies below the measured section indicating that the uppermost Permian Changhsingian and at least part of the Wuchiapingian stages postdate the end of the Permo–Carboniferous Reversed Superchron (PCRS). New age data from Shangsi reveal

that the age of the Illawarra reversal marking the end of the PCRS is over 260 Ma.

PT paralic mudstone and carbonate sediments from sections near Langdai, NW Guizhou Province span an R-N polarity sequence. Section-mean directions pass a fold test at the 95% confidence level, and the section-mean poles are close to the mean PT pole for the South China block. Correlating the R-N transition recorded at Langdai sections with that at Shangsi allows us to constrain the biotic crisis in the Langdai paralic PT sediments. Results from marine (Shangsi) and paralic (Langdai) sections are consistent, yielding an R-N transition that lies significantly below the biostratigraphically defined PT boundary, but coincident with the mass extinction horizon. To within the resolution of our sampling (~50 cm) there appears to be no lag in the timing of the inferred extinction boundary.

Paleomagnetic results from terrestrial sections in the southern Junggar basin are highly consistent, and yield a composite magnetostratigraphy containing three principal polarity chrons. A mismatch of marine (Shangsi) and terrestrial (Junggar) magnetostratigraphies, and recent palynologic data from the terrestrial sections, lead us to conclude that the PT boundary has been misplaced. While some ambiguity remains over the location of the biostratigraphic PT boundary in the Junggar sections, we interpret the PT-boundary to lie a significant distance (~150 m) below earlier interpretations.

Acknowledgments

We thank Bob Nicoll, Wang Xiaofeng, Wang Zhi-hao, Qu Xun, and Mao Xiaodong for their help in field sampling. We are grateful to Mark Hounslow and two anonymous reviewers whose comments helped to greatly improve the manuscript. This work was supported in part by grants from the Australian Research Council (# F39905954 to I. Metcalfe) and the National Science Foundation (EAR-#0125799 to R. Mundil and P. Renne). Laboratory work at the Berkeley Geochronology Center was supported by the Ann and Gordon Getty Foundation.

Appendix A. Supplementary data

Supplementary data associated with this article can be found in the online version, at doi:10.1016/j.jseae.2009.03.003.

References

- Avouac, J.-P., Tapponnier, P., Bai, M., You, H., Wang, G., 1993. Active thrusting and folding along the northern Tien Shan and late Cenozoic rotation of the Tarim relative to Dzungaria and Kazakhstan. *Journal of Geophysical Research, B Solid Earth and Planets* 98 (4), 6755–6804.
- Baud, A., Magaritz, M., Holser, W.T., 1989. Permian–Triassic of the Tethys; carbon isotope studies. *Geologische Rundschau* 78 (2), 649–677.
- Becker, L., Poreda, R.J., Hunt, A.G., Bunch, T.E., Rampino, M., 2001. Impact event at the Permian–Triassic boundary: evidence from extraterrestrial noble gases in fullerenes. *Science* 291 (5508), 1530–1533.
- Bowring, S.A., Erwin, D.H., Jin, Y.G., Martin, M.W., Davidek, K., Wang, W., 1998. U/Pb zircon geochronology and tempo of the end-Permian mass extinction. *Science* 280 (5366), 1039–1045.
- Carroll, A.R., 1998. Upper Permian lacustrine organic facies evolution, southern Junggar Basin, NW China. *Organic Geochemistry* 28 (11), 649–667.
- Chang, S., Renne, P.R., Mundil, R., 2007. Status report on the ⁴⁰Ar/³⁹Ar and U/Pb dating of tuffs in the Dewey Lake Formation of West Texas towards constraining the Permo–Triassic magnetostratigraphic time scale. 88(52) (Abstract V23B-1442).
- Courtillot, V., Jaupart, C., Manighetti, I., Tapponnier, P., Besse, J., 1999. On causal links between flood basalts and continental breakup. *Earth and Planetary Science Letters* 166 (3–4), 177–195.
- Courtillot, V.E., Renne, P.R., 2003. On the ages of flood basalt events. *Comptes Rendus Geoscience* 335 (1), 113–140.
- De Kock, M.O., Kirschvink, J.L., 2004. Paleomagnetic constraints on the Permian–Triassic boundary in terrestrial strata of the Karoo Supergroup, South Africa: implications for causes of the end-Permian extinction event. *Gondwana Research* 7 (1), 175–183.

- Erwin, D.H., 1993. The great Paleozoic crisis; life and death in the Permian. *Critical Moments in Paleobiology and Earth History Series*. Columbia University Press, New York. 327 pp.
- Farley, K.A., Ward, P., Garrison, G., Mukhopadhyay, S., 2005. Absence of extraterrestrial (super 3) He in Permian–Triassic age sedimentary rocks. *Earth and Planetary Science Letters* 240 (2), 265–275.
- Fisher, R.A., 1953. Dispersion on a sphere. *Proceedings of the Royal Society London* 217A, 295–305.
- Foster, C.B., Afonin, S.A., 2005. Abnormal pollen grains; an outcome of deteriorating atmospheric conditions around the Permian–Triassic boundary. *Journal of the Geological Society of London* 162 (4), 653–659.
- Foster, C.B., Stephenson, M.H., Marshall, C., Logan, G.A., Greenwood, P.F., 2002. A revision of *Reduviasporonites* Wilson 1962; description, illustration, comparison and biological affinities. *Palynology* 26, 35–58.
- Gallet, Y., Krystyn, L., Besse, J., Saidi, A., Ricou, L.E., 2000. New constraints on the Upper Permian and Lower Triassic geomagnetic polarity timescale from the Abadeh section (central Iran). *Journal of Geophysical Research-Solid Earth* 105 (B2), 2805–2815.
- Glikson, A., 2004. Comment on bedout: a possible end-Permian impact crater offshore of northwestern Australia. *Science* 306, 5296.
- Gurevitch, E., Westphal, M., DaraganSuchov, J., Feinberg, H., Pozzi, J.P., Khrumov, A.N., 1995. Paleomagnetism and magnetostratigraphy of the traps from Western Taimyr (northern Siberia) and the Permo-Triassic crisis. *Earth and Planetary Science Letters* 136 (3–4), 461–473.
- Haag, M., Heller, F., 1991. Late Permian to early Triassic magnetostratigraphy. *Earth and Planetary Science Letters* 107 (1), 42–54.
- Hagstrum, J.T., 2005. Antipodal hotspots and bipolar catastrophes; were oceanic large-body impacts the cause? *Earth and Planetary Science Letters* 236 (1–2), 13–27.
- Hallam, A., Wignall, P.B., 1999. Mass extinctions and sea-level changes. *Earth-Science Reviews* 48 (4), 217–250.
- Heller, F., Chen, H., Dobson, J., Haag, M., 1995. Permian–Triassic magnetostratigraphy; new results from South China. *Physics of the Earth and Planetary Interiors* 89 (3–4), 281–295.
- Heller, F., Lowrie, W., Li, H., Wang, J., 1988. Magnetostratigraphy of the Permo-Triassic boundary section at Shangsi (Guangyuan, Sichuan Province, China). *Earth and Planetary Science Letters* 88 (3–4), 348–356.
- Holser, W.T., Schonlaub, H.P., Attrep, M., Boeckelmann, K., Klein, P., Magaritz, M., Orth, C.J., Fenninger, A., Jenny, C., Kralik, M., Mauritsch, H., Pak, E., Schramm, J.M., Statterger, K., Schmoller, R., 1989. A unique geochemical record at the Permian Triassic boundary. *Nature* 337 (6202), 39–44.
- Hounslow, M.W., Mork, A., Peters, C., Weitschat, W., 1996. Boreal Lower Triassic magnetostratigraphy from Deltadalen, Central Svalbard. *Albertina* 17, 3–10.
- Irving, E., Parry, L.G., 1963. The magnetism of some Permian rocks from New South Wales. *Geophysical Journal* 7 (4), 395–411.
- Kaiho, K., Kajiwara, Y., Nakano, T., Miura, Y., Kawahata, H., Tazaki, K., Ueshima, M., Chen, Z., Shi, G.R., 2001. End-Permian catastrophe by a bolide impact; evidence of a gigantic release of sulfur from the mantle. *Geology* 29 (9), 815–818.
- Khrumov, A.N., 1974. *Palaeomagnetism of Palaeozoic*. Nedra, Leningrad.
- Kirschvink, J.L., 1980. The least-squares line and plane and the analysis of paleomagnetic data. *Geophysical Journal of the Royal Astronomical Society* 62, 699–718.
- Knoll, A.H., Bambach, R.K., Payne, J.L., Pruss, S., Fischer, W.W., 2007. Paleophysiology and end-Permian mass extinction. *Earth and Planetary Science Letters* 256, 295–313.
- Krull, E.S., Retallack, G.J., 2000. Delta C-13 depth profiles from paleosols across the Permian–Triassic boundary: evidence for methane release. *Geological Society of America Bulletin* 112 (9), 1459–1472.
- Lai, X., Yang, F., Hallam, A., Wignall, P.B., 1996. The Shangsi section, candidate of the global stratotype section and point of the Permian–Triassic boundary. In: Yin, H. (Ed.), *The Palaeozoic–Mesozoic Boundary: Candidates for the Global Stratotype Section and Point of the Permian–Triassic Boundary*. China University of Geosciences Press, Wuhan, pp. 113–124.
- Li, H., Wang, J., 1989. Magnetostratigraphy of Permo-Triassic boundary section of Meishan of Changxing, Zhejiang. *Scientia Sinica Series B* 32 (11), 1401–1408.
- Li, P.X., Zhang, Z.M., Wu, S.Z., 1986a. Stratigraphy. In: Yang, J. et al. (Eds.), *Permian and Triassic Strata and Fossil Assemblages in the Dalongkou area of Jimjar, Xinjiang*. Geol. Publ. House, Beijing, China, pp. 2–38.
- Li, Y.A., Li, J., Liu, Y.L., Zhang, Z.K., 1981. Paleomagnetic character of Permian–Triassic in Lucaogou of Urumqi. In: X.a.I.G. Inst. Geol., CAGS (Eds.), *Research on the Boundary Between Permian and Triassic in the Tianshan mountains of China*. China Ocean Press, Beijing, pp. 71–84.
- Li, Z., Zhan, L., Zhu, X., Zhang, J., Jin, R., Liu, G., Sheng, H., Shen, G., Dai, J., Huang, H., Xie, L., Yan, Z., 1986b. Mass extinction and geological events between the Paleozoic and Mesozoic eras. *Dizhixue Bao (Acta Geologica Sinica)* 60 (1), 1–17.
- Lowrie, W., 1990. Identification of ferromagnetic minerals in a rock by coercivity and unblocking temperature properties. *Geophysical Research Letters* 17, 159–162.
- Lozovsky, V.R., 1998. The Permian–Triassic boundary in the continental series of Eurasia. *Palaeogeography, Palaeoclimatology, Palaeoecology* 143 (4), 273–283.
- Lucas, S.G., 1998. Global Triassic tetrapod biostratigraphy and biochronology. In: Lucas, S.G., Yin, H. (Eds.), *Palaeogeography, Palaeoclimatology, Palaeoecology*, pp. 345–382.
- Machel, H.G., 1996. Magnetic contrasts as a result of hydrocarbon seepage and migration. *American Association of Petroleum Geologists Memoir* 66, 99–109.
- Mattinson, J.M., 2005. Zircon U–Pb chemical abrasion (“CA-TIMS”) method: Combined annealing and multi-step partial dissolution analysis for improved precision and accuracy of zircon ages. *Chemical Geology* 220 (1–2), 47–66.
- McFadden, P.L., 1990. A new fold test for palaeomagnetic studies. *Geophysical Journal International* 103 (1), 163–169.
- McFadden, P.L., McElhinny, M.W., 1988. The combined analysis of remagnetization circles and direct observations in paleomagnetism. *Earth and Planetary Science Letters* 87, 161–172.
- McFadden, P.L., McElhinny, M.W., 1990. Classification of the reversal test in palaeomagnetism. *Geophysical Journal International* 103, 725–729.
- Menning, M., 1995. A numerical time scale for the Permian and Triassic periods: an integrative time analysis. In: Scholle, P.A., Peryt, T.M., Ulmer-Scholle, D.S. (Eds.), *The Permian of Northern Pangea*. Springer-Verlag, pp. 77–97.
- Metcalfe, I., Mundil, R., Nicoll, R.S., Foster, C., Glen, J., Lyons, J., Xiaofeng, W., Cheng-Yuan, W., Nomade, S., Renne, P.R., Black, L., Xun, Q., Xiaodong, M., 2003. Age and correlation of the Permian–Triassic boundary & mass extinction in China. In: *Proceedings of the 25th International Congress on Carboniferous and Permian Stratigraphy and Fifty Fifth Meeting of the International Committee for Coal and Organic Petrology – ICCP, Utrecht, The Netherlands*, pp. 352–353.
- Metcalfe, I., Nicoll, R.S., 2007. Conodont biostratigraphic control on transitional marine to non-marine Permian–Triassic boundary sequences in Yunnan–Guizhou, China. *Palaeogeography, Palaeoclimatology, Palaeoecology* 252, 56–65.
- Metcalfe, I., Nicoll, R.S., Mundil, R., Foster, C., Glen, J., Lyons, J., Wang, X.F., Wang, C.Y., Renne, P.R., Black, L., Xun, Q., Mao, X.D., 2001. The Permian–Triassic boundary and mass extinction in China. *Episodes* 24 (4), 239–244.
- Metcalfe, I., Nicoll, R.S., Wardlaw, B.R., 2007. Conodont index fossil *Hindeodus changxingensis* Wang fingers greatest mass extinction event. *Palaeoworld* 16, 202–207.
- Min, K., Mundil, R., Renne, P.R., Ludwig, K.R., 2000. A test for systematic errors in ⁴⁰Ar/³⁹Ar geochronology through comparison with U/Pb analysis of a 1.1-Ga rhyolite. *Geochimica et Cosmochimica Acta* 64 (1), 73–98.
- Molina-Garza, R.S., Geissman, J.W., Van der Voo, R., 1989. Paleomagnetism of the Dewey Lake formation (Late Permian), Northwest, Texas: end of the Kiaman Superchron in North America. *Journal of Geophysical Research* 94, 17881–17888.
- Morante, R., 1996. Permian and Early Triassic isotopic records of carbon and strontium in Australia and a scenario of events about the Permian–Triassic boundary. *Historical Biology* 11, 289–310.
- Müller, R.D., Goncharov, A., Kritski, A., 2005. Geophysical evaluation of the enigmatic Bedout basement high, offshore northwestern Australia. *Earth and Planetary Science Letters* 237 (1–2), 264–284.
- Mundil, R., Ludwig, K.R., Metcalfe, I., Renne, P.R., 2004. Age and timing of the Permian mass extinctions: U/Pb dating of closed-system zircons. *Science* 305 (5691), 1760–1763.
- Mundil, R., Metcalfe, I., Chang, S., Renne, P.R., 2006a. The Permian–Triassic boundary in Australia; new radio-isotopic ages. *Geochimica et Cosmochimica Acta* 70, A436.
- Mundil, R., Metcalfe, I., Ludwig, K.R., Renne, P.R., Oberli, F., Nicoll, R.S., 2001. Timing of the Permian–Triassic biotic crisis: implications from new zircon U/Pb age data (and their limitations). *Earth and Planetary Science Letters* 187 (1–2), 131–145.
- Mundil, R., Renne, P.R., Min, K.K., Ludwig, K.R., 2006b. Resolvable miscalibration of the (super 40)Ar/(super 39)Ar geochronometer [modified]. *Eos, Transactions, American Geophysical Union*, 87 (Abstract V21A-0543).
- Nawrocki, J., 1997. Permian to Early Triassic magnetostratigraphy from the Central European Basin in Poland: implications on regional and worldwide correlations. *Earth and Planetary Science Letters* 152 (1–4), 37–58.
- Nawrocki, J., 2004. The Permian–Triassic boundary in the Central European Basin: magnetostratigraphic constraints. *Terra Nova* 16 (3), 139–145.
- Nicoll, R.S., Metcalfe, I., Wang, C., 2002. New species of the conodont genus *Hindeodus* and the conodont biostratigraphy of the Permian–Triassic boundary interval. *Journal of Asian Earth Sciences* 20 (6), 609–631.
- Nie, S., Rowley, D.B., Van der Voo, R., Li, M., 1993. Paleomagnetism of late Paleozoic rocks in the Tianshan, northwestern China. *Tectonics* 12 (2), 568–579.
- Ogg, J.G., Steiner, M.B., 1991. Early Triassic magnetic polarity time scale integration of magnetostratigraphy, ammonite zonation and sequence stratigraphy from stratotype sections (Canadian Arctic Archipelago). *Earth and Planetary Science Letters* 107 (1), 69–89.
- Ouyang, S., Norris, G., 1999. Earliest Triassic (Induan) spores and pollen from the Junggar Basin, Xinjiang, northwestern China. *Review of Palaeobotany and Palynology* 106 (1–2), 1–56.
- Payne, J.L., Lehmann, D.J., Follett, D., Seibel, M., Kump, L.R., Riccardi, A.L., Altiner, D., Sano, H., Wei, J., 2007. Erosional truncation of uppermost Permian shallow-marine carbonates and implications for Permian–Triassic boundary events. *Geological Society of America Bulletin* 119 (7–8), 771–784.
- Peng, Y.Q., Zhang, S.X., Yu, T.X., Yang, F.Q., Gao, Y.Q., Shi, G.R., 2005. High-resolution terrestrial Permian–Triassic eventostratigraphic boundary in western Guizhou and eastern Yunnan, southwestern China. *Palaeogeography, Palaeoclimatology, Palaeoecology* 215 (3–4), 285–295.
- Prevot, M., Mankinen, E.A., Gromme, S., Lacaille, A., 1983. High paleointensities of the geomagnetic field from thermomagnetic studies on rift valley pillow basalts from the Mid-Atlantic Ridge. *Journal of Geophysical Research* 88 (B3), 2316–2326.
- Rampino, M.R., 1992. A major Late Permian impact event on the Falkland Plateau. *Eos, Transactions, American Geophysical Union* 73, 336.

- Raup, D.M., 1979. Size of the Permo-Triassic bottleneck and its evolutionary implications. *Science* 206 (4415), 217–218.
- Rees, P.M., 2002. Land-plant diversity and the end-Permian mass extinction. *Geology* 30 (9), 827–830.
- Reichow, M.K., Saunders, A.D., White, R.V., Pringle, M.S., Al'Mukhamedov, A.I., Medvedev, A.I., Kirida, N.P., 2002. $^{40}\text{Ar}/^{39}\text{Ar}$ dates from the West Siberian Basin: Siberian flood basalt province doubled. *Science* 296 (5574), 1846–1849.
- Renne, P.R., 1995. Excess ^{40}Ar in biotite and hornblende from the Noril'sk 1 Intrusion, Siberia; implications for the age of the Siberian Traps. *Earth and Planetary Science Letters* 131 (3–4), 165–176.
- Renne, P.R., Basu, A.R., 1991. Rapid eruption of the Siberian Traps flood basalts at the Permo-Triassic boundary. *Science* 253 (5016), 176–179.
- Renne, P.R., Melosh, H.J., Farley, K.A., Reimold, W.U., Koeberl, C., Rampino, M.R., Kelly, S.P., Ivanov, B.A., 2004. Is Bedout an impact crater? Take 2. *Science* 306 (5296), 610–611.
- Renne, P.R., Zhang, Z., Richards, M.A., Black, M.T., Basu, A.R., 1995. Synchrony and causal relations between Permian–Triassic boundary crises and Siberian flood volcanism. *Science* 269 (5229), 1413–1416.
- Renne, P.R., Zhou, Z., Nomade, S., Mundil, R., Metcalfe, I., 2004b. The time scale of extinctions and paleoenvironmental crisis from $^{40}\text{Ar}/^{39}\text{Ar}$ dating of Permo-Triassic bentonites at Shangsi (Schizuan, China). *American Association of Petroleum Geologists* 32, Florence, p. 964.
- Rohde, R.A., Muller, R.A., 2005. Cycles in fossil diversity. *Nature* 434 (7030), 208–210.
- Ryskin, G., 2003. Methane-driven oceanic eruptions and mass extinctions. *Geology* 31 (9), 741–744.
- Scholger, R., Mauritsch, H.J., Brandner, R., 2000. Permian–Triassic boundary magnetostratigraphy from the Southern Alps (Italy). *Earth and Planetary Science Letters* 176 (3–4), 495–508.
- Sharps, R., Li, Y., McWilliams, M., Li, Y., 1992. Paleomagnetic investigations of Upper Permian sediments in the South Junggar Basin, China. *Journal of Geophysical Research* 97 (B2), 1753–1765.
- Steiner, M., Ogg, J., Zhang, Z., Sun, S., 1989. The Late Permian/Early Triassic magnetic polarity time scale and plate motions of South China. *Journal of Geophysical Research B: Solid Earth and Planets* 94 (6), 7343–7363.
- Steiner, M.B., 2006. The magnetic polarity time scale across the Permian–Triassic boundary. In: Lucas, S.G., Cassinis, G., Schneider, J.W. (Eds.), *Non-Marine Permian Biostratigraphy and Biochronology*. Geological Society of London Special Publications, pp. 15–38.
- Steiner, M.B., Eshet, Y., Rampino, M.R., Schwindt, D.M., 2003. Fungal abundance spike and the Permian–Triassic boundary in the Karoo Supergroup (South Africa). *Palaeogeography Palaeoclimatology Palaeoecology* 194 (4), 405–414.
- Szurliés, M., Bachmann, G.H., Menning, M., Nowaczyk, N.R., Kaeding, K.C., 2003. Magnetostratigraphy and high-resolution lithostratigraphy of the Permian–Triassic boundary interval in central Germany. *Earth and Planetary Science Letters* 212 (3–4), 263–278.
- Wang, K., Geldsetzer, H.H.J., Krouse, H.R., 1994. Permian–Triassic extinction; organic delta ^{13}C evidence from British Columbia, Canada. *Geology* 22 (7), 580–584.
- Ward, P.D., Botha, J., Buick, R., De Kock, M.O., Erwin, D.H., Garrison, G.H., Kirschvink, J.L., Smith, R., 2005. Abrupt and gradual extinction among Late Permian land vertebrates in the Karoo Basin, South Africa. *Science* 307 (5710), 709–714.
- Wardlaw, B.R., Davydov, V., Gradstein, F.M., 2004. The Permian period. In: Gradstein, F.M., Ogg, J.G., Smith, A.G. (Eds.), *A Geologic Time Scale 2004*. University Press, Cambridge, pp. 249–270.
- Wignall, P., Thomas, B., Willink, R., Watling, J., 2004. Is Bedout an impact crater? Take 1. *Science* 306 (5296), 609.
- Wignall, P.B., Hallam, A., Lai, X., Yang, F., 1995. Palaeoenvironmental changes across the Permian/Triassic boundary at Shangsi (N Sichuan, China). *Historical Biology* 10, 175–189.
- Wignall, P.B., Morante, R., Newton, R., 1998. The Permo-Triassic transition in Spitsbergen: Delta C-13(org) chemostratigraphy, Fe and S geochemistry, facies, fauna and trace fossils. *Geological Magazine* 135 (1), 47–62.
- Wignall, P.B., Twitchett, R.J., 1996. Oceanic anoxia and the end Permian mass extinction. *Science* 272 (5265), 1155–1158.
- Xu, D.-Y., Yan, Z., 1993. Carbon isotope and iridium event markers near the Permian/Triassic boundary in the Meishan section, Zhejiang Province, China. *Palaeogeography, Palaeoclimatology, Palaeoecology* 104, 171–175.
- Yang, Z., Besse, J., 2001. New Mesozoic apparent polar wander path for South China; tectonic consequences. *Journal of Geophysical Research* 106 (B5), 8493–8520.
- Yang, Z.Y., Yin, H.F., Wu, S.B., Yang, F.Q., Ding, M.H., Xu, G.R., 1987. Permian–Triassic boundary stratigraphy and fauna of South China. *China Ministry of Geology and Mineral Resources Geological Memoirs*. Geological Publishing House, Beijing (Series 2, Number 6).
- Yin, H., Sweet, W.C., Glenister, B.F., Kotlyar, G., Kozur, H., Newell, N.D., Sheng, J., Yang, Z., Zakharov, Y.D., 1996. Recommendation of the Meishan section as global stratotype section and point for basal boundary of Triassic System. *Newsletters on Stratigraphy* 34 (2), 81–108.
- Yin, H.F., Zhang, K.X., Tong, J.N., Yang, Z.Y., Wu, S.B., 2001. The global stratotype section and point (GSSP) of the Permian–Triassic boundary. *Episodes* 24 (2), 102–114.
- Zakharov, Y.D., Sokarev, A.N., 1991. Permian–Triassic paleomagnetism of Eurasia. In: *Proceedings of the International Symposium on Shallow Tethys*, vol. 3, pp. 313–323.
- Zhu, Y., Liu, Y., 1999. Magnetostratigraphy of the Permo-Triassic boundary section at Meishan, Changxing, Zhejiang Province. In: Yin, H., Tong, J. (Eds.), *Proceedings of the International Conference on Pangea and the Paleozoic–Mesozoic Transition*. China University of Geosciences Press, Wuhan, pp. 79–84.